Journal of Soils and Sediments (2022) 22:859–888
https://doi.org/10.1007/s11368-021-03082-y

SOILS, SEC 5 • SOIL AND LANDSCAPE ECOLOGY • RESEARCH ARTICLE

Investigation on desiccation cracking behavior of clayey soils with a perspective of fracture mechanics: a review

Jin-Jian Xu[1] · Chao-Sheng Tang[1] · Qing Cheng[1] · Qi-liang Xu[1] · Hilary I. Inyang[1,2,3] · Zhu-Yuan Lin[1] · Bin Shi[1]

Received: 10 August 2021 / Accepted: 30 September 2021 / Published online: 9 November 2021

Abstract

Purpose Soil cracking is a common natural phenomenon. The existence of soil cracks has significant effects on the engineering properties of clayey soil, and can cause significant problems in geotechnical, geological, and environmental aspects. Understanding of the potential mechanisms of soil cracking is essential in assessments of potential damages to earthen infrastructures.

Materials and method We review the past research efforts devoted to the experimental investigations and applications of fracture mechanics in soil cracking, attempting to provide a better understanding of the formation mechanism of desiccation cracking with a perspective of fracture mechanics.

Results and discussion This review analyzes the influence of soil cracking on soil engineering properties and the significance of soil cracking phenomena. Past and current formulations of soil fracture criteria and their experimental investigation are discussed. This review reveals the factors that affect the mechanisms of soil fracture can be divided into two groups, namely soil intrinsic properties and test-related factors. The applications of fracture mechanics in soil cracking are also discussed with particular focus on soil fracture models that are separately based on linear elastic fracture mechanics (LEFM), elastic plastic fracture mechanics (EPFM), and numerical simulations of soil cracking based on fracture mechanics. **S**ome challenges and prospects of the applications of fracture mechanics in soil cracking are presented.

Conclusions Fracture mechanics is a significant method to explain soil crack initiation and propagation. It is expected that researchers can gain better understanding of the range of fracture mechanics applications in soil cracking, and seek improvements and extensions of existing models through this review.

Keywords Soil cracking · Fracture mechanics · Soil fracture parameters · Fracture criterion · Fracturing influencing factors · Theoretical model · Numerical simulation

1 Introduction

Some global regions have become more arid due to climate change. Desiccation cracking of soil is a common phenomenon in such regions. The formation of soil desiccation cracks

Responsible editor: by Lu Zhang

✉ Chao-Sheng Tang
tangchaosheng@nju.edu.cn

✉ Qing Cheng
chengqing@nju.edu.cn

Jin-Jian Xu
Xujianjian@smail.nju.edu.cn

Hilary I. Inyang
h.inyang26@gmail.com

Zhu-Yuan Lin
crecyslin@smail.nju.edu.cn

Bin Shi
shibin@nju.edu.cn

[1] School of Earth Sciences and Engineering, Nanjing University, 163 Xianlin Road, Nanjing 210023, China

[2] Global Education and Infrastructure Services Inc., Charlotte, NC, USA

[3] Bahir Dar University, Bahir Dar, Ethiopia

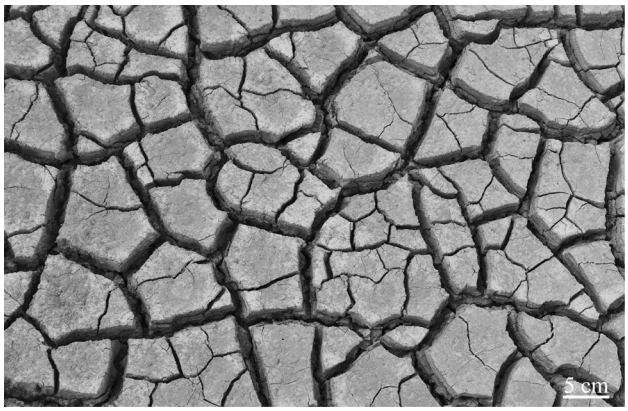

Fig. 1 Drying-induced soil cracking in natural environment

due to moisture evaporation and volumetric shrinkage is frequently observed in drying climatic regions (Fig. 1). The existence of soil cracks has significant effects on the engineering properties of clayey soil, and can cause significant problems in geotechnical, geological and environmental aspects (Corte and Higashi 1960; Albrecht and Benson 2001; Sanchez et al. 2013; Tang et al. 2008; Tollenaar et al. 2017; Song and Cui 2020). Soil cracking enlarges soil macropore sizes, thereby, changing soil internal structure and hydraulic properties by creating preferential flow paths for the migration of moisture and contaminants (Albrecht and Benson 2001; Zhang et al. 2016; Abd El-Halim 2017; Tang et al. 2019; Wei et al. 2020; Xu et al. 2020; Colombi et al. 2021). The development of soil cracks can increase the hydraulic conductivity drastically and facilitate water infiltration, which will lead to failure of waste containment structures (Li and Zhang 2010, 2011). Water infiltration will change porewater pressure in unsaturated soils, thereby affecting the soil shear strength. In addition, cracks can form part of a slip surface that has no shear strength. (Li et al. 2011, 2017). Since clayey soils are widely used as impermeable layers for the landfill and waste isolation near the ground surface, soil cracks can greatly increase the hydraulic conductivity, which may cause the leakage of contamination and increase the risk of environmental pollution (Omidi et al. 1996; Miller et al. 1998; Hewitt and Philip 1999; Rayhani et al. 2007; Narani et al. 2020). Moreover, soil cracking increases clayey slope weathering depth and surface roughness. This aggravates soil erosion on the slope surfaces and also reduces soil cohesion, leading to slope instability (Baker 1981; Fredlund 1987; Alonso et al. 1995; Krisnanto et al. 2014; Wang et al. 2018a; Di Carlo et al. 2019; Poulsen et al. 2020; Stirling et al. 2020). Existence of soil cracks can degrade hydraulic-physical properties of earth structures (e.g., levee, slope and landfill), and can result in catastrophic failures as presented in Fig. 2. For example, there are thousands of kilometers of levees that have cracked in several countries, including the UK, the Netherlands, and the USA under seasonal drought conditions (Vahedifard et al. 2016). Billions of dollars have to be expended to repair cracked levees to prevent piping and direct levee failure every year (Robinson and Vahedifard 2016). Understanding of the potential mechanisms of soil cracking is essential in assessments of potential damages to infrastructures (Peron et al. 2009b; Cordero et al. 2017; Murray and Tarantino 2019; Wei et al. 2016, 2020).

Currently, research methods used in analyses of soil cracking include laboratory tests, field tests and numerical simulations. In laboratory tests, soil cracking is

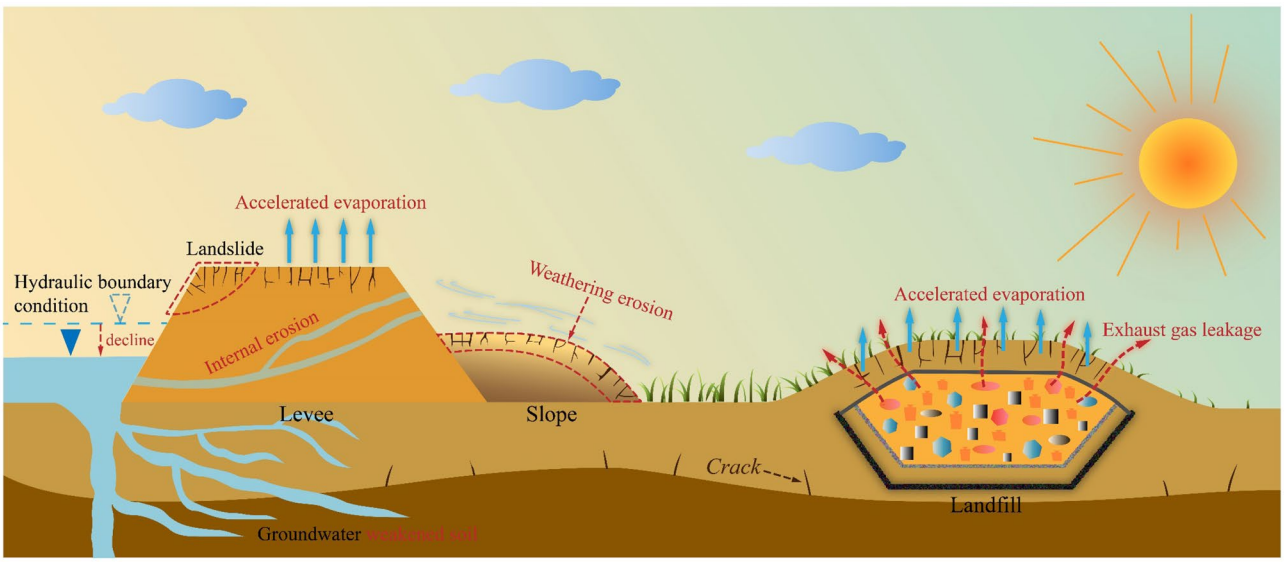

Fig. 2 Potential undermining mechanisms imposed on the levee, slope and landfill due to drought-induced soil cracking

controlled by a large number of factors, including temperature, thickness of soil layer, drying-wetting cycles, boundary effects and other experimental conditions (Tang et al. 2008, 2011a, 2013; Costa et al. 2013a; Xing et al. 2017; Lakshmikantha et al. 2018; Zeng et al. 2019). To study thermal effects on the soil desiccation cracking, Tang et al. (2008) performed desiccation experiments on a Nanjing area clayey soil. The soil cracking patterns obtained under different temperature conditions (30, 40, 50 ℃) were quantitatively indexed for comparison. The results showed that crack length, width, aggregate area increase with increasing temperature. Similar observations were made on other studied by Tang et al. (2011a). In order to analyze the influence of soil layer thickness on soil cracking, Zeng et al. (2019) analyzed clayey soil from Nanjing City. Saturated slurry samples were made with different soil layer thicknesses (0.5 cm, 1.0 cm, 1.5 cm). After drying, the crack total length, crack numbers, clod numbers and crack segment numbers were found to decrease with increase in soil thickness while the soil surface crack ratio and crack average width displayed on the opposite trend. Soil cracking during different wetting–drying cycles has been investigated in a number of studies (Wang et al. 2017; Albrecht 2001; Tang et al. 2011b). Wang et al. (2017) investigated the geometric and fractal features of soil cracking patterns using a digital camera on compacted soil samples subjected to four wetting–drying cycles. It was found that the crack networks of samples tend to be stable as the number of wetting–drying cycles increases and the crack patterns are mainly affected by the first cracking incident in the subsequent wetting–drying cycles. The same phenomenon has also been observed by other researchers (Albrecht 2001; Tang et al. 2011b; Wang et al. 2017, 2018b; Julina and Thyagaraj 2020). Moreover, effects of boundary conditions (i.e., sample sizes, shapes, and aspect ratios of specimens and containers) on the development of crack processes and the final crack patterns have been investigated (Lakshmikantha et al. 2018; Qu et al. 2020; Al-Jeznawi et al. 2021).

Due to large differences between experimental conditions of laboratory tests and the natural environment, the reliability and representativeness of the laboratory tests on soil cracking has often drawn controversy. Meanwhile, small-size laboratory tests may not represent well field conditions where the soil often contains coarse particles and structures, and has strong interactions with the atmosphere (Li and Zhang 2011a). Therefore, it is necessary to perform field experiments to verify natural soil crack patterns. However, the latter approach is hampered by high operation costs, time and effort inputs, and uncontrollable environmental conditions. For these reasons, few field studies on soil desiccation tests have been reported so far. Konrad and Ayad (1997a) excavated soil layers at three different levels and exposed them to continuous evaporation for 35 days. In order to assess cracking mechanisms, they observed and recorded the crack initiation and formation process of soil cracks in the topsoil layer, a weathered clay crust, and an intact clay. Abou Najm et al. (2010) conducted a 54-day field experiment on a farmland to monitor the evolution of surface cracks using digital imagery and 3-D visualization of the preferential flow paths network in soils using liquid latex. Li and Zhang (2010) investigated the field crack patterns and probability distributions of the geometric parameters of cracks and to determine the representative elementary volume (REV) of the crack network. Li and Zhang (2011) performed a 2-year field experiment to study the mechanisms of desiccation crack development in residual soils and backfill of road slopes. It was found that the crack pattern is closely related to the water content and drying time of the in-situ soil materials. Yu et al. (2021) conducted a desiccation crack monitoring campaign on a full-scale, vegetated infrastructure embankment subjected to 1-year of seasonally variable weather and pointed out the distribution of cracking was heavily related to prevailing wind direction (exposure) and crack response is driven by seasonal changes in meteorological and soil hydrological conditions.

As regards numerical simulation, Peron et al. (2009a) developed a two-dimensional Discrete Element Method (DEM) to study mud crack patterns under free boundary and constrained boundary conditions. The model was able to capture crack initiation, extension and final geometric morphology. Shin and Santamarina (2011) used a Finite Element Method (FEM) model to capture crack growth based on an effective-stress formulation, which follows only mode I tensile failure and is not able to account for crack interactions. Sima et al. (2014) proposed an approach to modeling of soil cracking in thin clay layers based on DEM, which could successfully capture the formation and development of cracks during drying. Hirobe and Oguni (2017) proposed a mathematical model to simulate patterns of soil cracks. This coupled model that they developed includes three aspects: desiccation, deformation, and fracture and is able to recast the basic features of the crack geometry. Lin et al. (2020) used DEM to simulate desiccation cracks initiated from both the top surface and the bottom in thin soil layers.

Although researchers have studied soil cracking processes and resulting crack patterns by different methods including laboratory tests, field tests and numerical simulations, no parameter can solely explain the soil cracking mechanism. Soil is a complicated, multi-phase granular material, and its cracking behavior is governed by several factors that defy the competence of any unified theoretical model in soil mechanics or fracture mechanics as regards soil crack initiation and propagation. In this review, the latest findings on the contribution of fracture mechanics to the analyses of soil cracking mechanism are presented in seven sections as

follows: Section 1 expounds the significance of studying soil cracking and points out the lack of soil cracking mechanics models. Section 2 briefly introduces the fracture criterion of soil fracture parameters. Section 3 summarizes the past and existing experimental investigations of soil fracturing, including three-point bending test, four-point bending test, compact tension test, ring test, and compression test. Section 4 categorizes major factors that affect soil fracturing parameters into two groups, covering soil intrinsic properties and test-related factors. Section 5 discusses existing soil cracking models based on LEFM and EPFM. Section 6 describes numerical simulations of soil cracking based on fracture mechanics with primary focus on LEFM model and the cohesive crack method. Finally, a brief summary of concluding remarks and some prospects that require further investigations are presented in Sect. 7. Through this review, it is expected that researchers can better appreciate opportunities for adaptation of fracture mechanics principles for prediction of fracture patterns and development remedial measures for threatened natural and constructed systems.

2 Fracture criterion and soil fracture parameters

Over the past few decades, the field of fracture mechanics has undoubtedly prevented a substantial number of structural failures (Goehring et al. 2015). Fracture mechanics, known as the mechanics of cracked body, is the main tool for studies of cracking processes and behavior of materials. Heretofore, the development of fracture mechanics has focused on brittle and quasi-brittle materials such as concrete and rock (Cai et al. 1990; Scavia 1990; Han et al. 2018; Guan et al. 2019; Lau et al. 2019; Khalilpour et al. 2019), it has also been used to analyze the cracking of hardened soils. Skempton et al. (1969) and Bishop (1971) were the first researchers to utilize fracture mechanics to analyze the progressive failure of slopes composed of stiff but cracked clay, an approach that was followed up by Vallejo (1994). Konrad and Ayad (1997b) proposed a highly idealized analytical model based on LEFM, for predicting the spacings among the soil desiccation cracks and describing crack propagation. Numerous beam bending tests and compact tension tests have been performed on soil specimens to investigate the relationship between fracture toughness and tensile strength or other mechanical properties of soil (Wang et al. 2007a, 2007b; Lakshmikantha et al. 2008, 2012).

In fracture mechanics, cracks can be divided into single-mode cracks and mixed-mode cracks. The single mode fracture can be divided into three basic modes (Chaves et al. 2014; Wu et al. 2017): mode I (opening mode), mode II (shearing mode) and mode III (tearing mode), as illustrated in Fig. 3. In the Opening mode, the external load is the normal stress in the vertical crack plane. The relative displacement of the crack faces is perpendicular to the crack plane, which usually occurs when the load and geometry are symmetrical to the crack plane. In the Shearing mode, the external load is the in-plane shear stress parallel to the crack faces and perpendicular to the crack front. The crack slides perpendicular to the front edge of the crack in its own plane. In the Tearing mode, the external load is the out-of-plane shear stress parallel to the crack faces and parallel to the front edge of the crack. The crack displaces parallel to the front edge of the crack in its own plane. The mixed mode is a combination of two or the all three basic modes, and most of actual engineering cracks are mixed mode cracks.

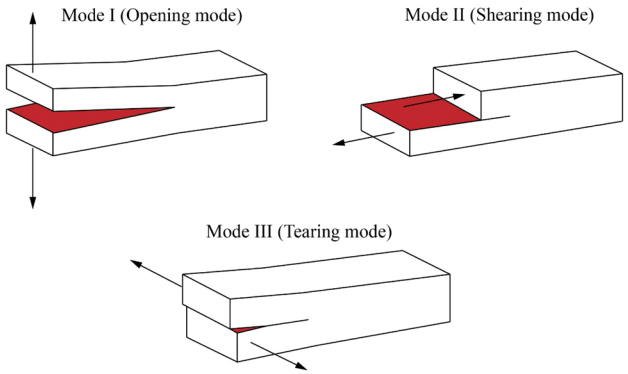

Fig. 3 Three modes of cracking

In order to understand the soil cracking behavior based on fracture mechanics, it is important to presage the soil fracture parameters and corresponding fracture criteria. The primary soil fracture parameters are fracture toughness K_C, critical energy release rate G_C, J integral J_C, crack tip opening displacement $CTOD$, critical maximum hoop stress $\sigma_{\theta maxC}$ and critical strain energy density factor S_C. Fracture criteria that are based on the parameters listed above can be used to determine the initiation and development of soil cracks.

2.1 Fracture toughness K_C

Irwin (1957) proposed that crack propagation is related to the stress field near the crack tip and that the stress intensity factor can be used in setting the fracture criterion. This principle has been widely used in engineering practice till date. The stress field of the crack tip is illustrated in Fig. 4a. Essentially, K_I, K_{II} and K_{III} are the stress intensity factors of mode I, II ,III cracks, which can be expressed as Eq. (1):

$$\begin{cases} K_I = \lim\limits_{r\to 0}\sqrt{2\pi r}\sigma_y(r,0) \\ K_{II} = \lim\limits_{r\to 0}\sqrt{2\pi r}\tau_{xy}(r,0) \\ K_{III} = \lim\limits_{r\to 0}\sqrt{2\pi r}\tau_{yz}(r,0) \end{cases} \tag{1}$$

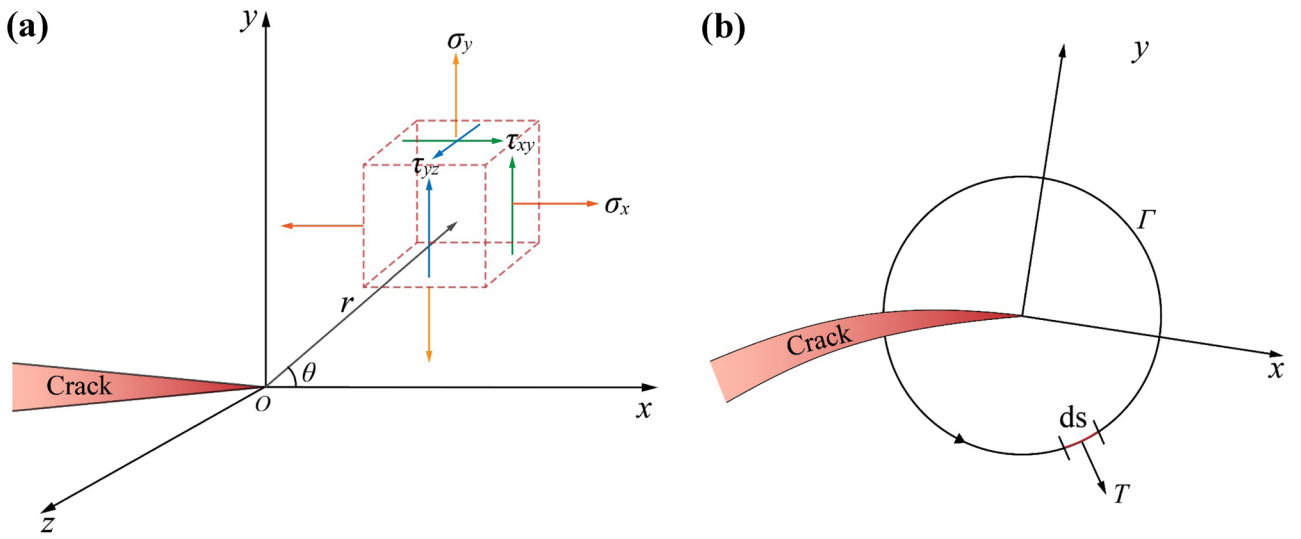

Fig. 4 (**a**) Stress field of the crack tip, (**b**) the integration path of J integral

It is intuitive to find from Eq. (1) that the stress intensity factor K is related to the crack stress and length and increases with increase in stress. Soil cracks will rapidly propagate from the original state when the critical condition is exceeded. Commonly used methods for determining stress intensity factors are analytical methods, numerical calculation methods and experimental methods. The fracture criteria of modes I, II, III crack can be expressed as Eq. (2) based on stress intensity factors:

$$\begin{cases} K_I \geq K_{IC} \\ K_{II} \geq K_{IIC} \\ K_{III} \geq K_{IIIC} \end{cases} \tag{2}$$

where K_{IC} K_{IIC}, K_{IIIC} are the fracture toughness of mode I, II, III crack, respectively. Fracture toughness is a unique property of the material itself. It characterizes the resistance of the material to cracking.

2.2 Critical energy release rate G_C

The energy release rate G is an important parameter for analyzing soil cracking from an energy perspective, and refers to the energy released when a crack expands per unit area. The relationship between the energy release rate and the stress intensity factor can be obtained by analyzing the stress field at the crack tip from an energy perspective. It is can be expressed as Eq. (3):

$$\begin{cases} G_I = \frac{1-\nu^2}{E} K_I^2 \\ G_{II} = \frac{1-\nu^2}{E} K_{II}^2 \\ G_{III} = \frac{1+\nu}{E} K_{III}^2 \end{cases} \tag{3}$$

where E is the elastic modulus, v is the Poisson's ratio. For the mixed-mode crack, the energy release rate is expressed as:

$$G = \frac{1-\nu^2}{E} K_I^2 + \frac{1-\nu^2}{E} K_{II}^2 + \frac{1+\nu}{E} K_{III}^2 \tag{4}$$

The fracture criterion based on energy release rate can be expressed as Eq. (5):

$$G \geq G_C \tag{5}$$

2.3 J integral J_C

Cherepanov (1967) and Rice (1968) independently proposed an integral method that is independent of the integration path in elasto-plastic fracture mechanics, named J integral. It is used to comprehensively measure the stress–strain field strength at the crack tip. The J integral explains the change in potential energy due to crack propagation. This theory avoids the direct calculation of the elasto-plastic stress and strain fields near the crack tip and applies the far-field J integral as the average parameter of the stress–strain concentration characteristics of the crack tip. For the two-dimensional problems, J integral can be defined as:

$$J = \int_{\Gamma} \left(W dy - T_i \frac{\partial u_i}{\partial x} ds \right) \tag{6}$$

where Γ is a simple integration path from a point on the lower surface of the crack to a point on the upper surface of the

crack; W is the elastoplastic strain energy density; T_i is the principal stress acting on the unit perimeter of the integration circuit; u_i is the displacement on the boundary of the integral circuit; x is the cartesian coordinate; ds is the arc length of the integral circuit, as shown in Fig. 4b. It can be proved analytically that the J integral has nothing to do with the selection of the integral route Γ, that is, the J integral satisfies the path conservation. The J integral has a clear physical meaning, which represents the energy release rate of the crack when it grows along the x direction per unit length.

The fracture criterion based on J integral is expressed by Eq. (7):

$$J \geq J_C \tag{7}$$

where J_C is the strain fracture toughness of the crack during crack initiation. Per the principles of LEFM, it can be proven that the J integral, the energy release rate G, and the stress intensity factor K satisfy the following relationship:

$$J = G = \frac{K_I^2 + K_{II}^2}{E} + \frac{1+\nu}{E} K_{III}^2 \tag{8}$$

2.4 Crack tip opening displacement CTOD

Wells (1961) first proposed a fracture criterion that is based on *CTOD* and is expressed as a certain deformation dimension of the crack tip. The *CTOD* is a macroscopic parameter and is defined as the displacement between the crack faces of a loaded ideal crack. The fracture criterion based on crack tip opening displacement is expressed as Eq. (9):

$$\delta \geq \delta_C \tag{9}$$

where δ is the crack tip opening displacement; δ_C is the critical crack tip opening displacement, which is not only equivalent to the crack propagation resistance, but also a constant parameter of the material elastic–plastic fracture toughness. The specific definition of *CTOD* depends on which point of the crack faces is used for calculation. The representative definition methods mainly include the following:

Due to the material follows the linear elastic constitutive relation, the displacement field of the mode I crack tip can be obtained by elastic mechanics:

$$\begin{cases} u = \frac{K_I}{2G}\sqrt{\frac{r}{2\pi}}cos\frac{\theta}{2}\left(\kappa - 1 + 2\sin^2\frac{\theta}{2}\right) \\ \upsilon = \frac{K_I}{2G}\sqrt{\frac{r}{2\pi}}sin\frac{\theta}{2}\left(\kappa + 1 - 2\cos^2\frac{\theta}{2}\right) \end{cases} \tag{10}$$

where u and υ are the displacement components in the x and y directions; G is the shear modulus; the relationship between κ and Poisson's ratio ν is expressed as Eq. (11):

$$\kappa = \begin{cases} 3 - 4\nu & Plaine\ strain \\ \frac{3-\nu}{1+\nu} & Plane\ stress \end{cases} \tag{11}$$

while $\theta = +\pi \in$ on the crack faces:

$$u = 2\upsilon = \frac{\kappa + 1}{G}\frac{K_I\sqrt{r}}{\sqrt{2\pi}} \tag{12}$$

Irwin (1957) first gave a preliminary estimate of the plastic zone size at the mode I crack tip. The tensile stress in r^* at crack tip just reaches the yield strength σ_{ys} where r^* is the size of the plastic zone, which can be calculated as:

$$r^* = \frac{K_I^2}{2\pi\sigma_{ys}^2} \tag{13}$$

With the modification of the Irwin plastic zone, the true crack length is replaced by the effective crack length. Consequently, the origin moves to the tip of the effective crack, as shown in Fig. 5a. Therefore, the corrected *CTOD* value can be expressed as:

$$\delta = \frac{4K_I^2}{\pi E\sigma_{ys}} \tag{14}$$

Similarly, the effective crack length can also be obtained by the method that Dugdale (1960) proposed, as presented in Fig. 5b. The *CTOD* calculated by Dugdale method, is:

$$\delta = \frac{8\sigma_{ys}a}{\pi E} ln\left(\sec\left(\frac{\pi\sigma}{2\sigma_{ys}}\right)\right) \tag{15}$$

where a is the crack length, (σ) is the far-field tensile load.

The definition of CTOD and CTOA is the crack tip opening displacement and the crack tip opening angle, respectively. CTOD (or CTOA) has become a reliable and convenient fracture criterion to assess crack extension and directionality in materials. Many materials have been found to exhibit a constant critical CTOD (or CTOA) from crack initiation through failure, making CTOD (or CTOA) a useful and reliable fracture criterion (Newman et al. 2003; Zhu and Joyce 2012).

2.5 Critical maximum hoop stress $\sigma_{\theta maxC}$

The maximum hoop stress criterion is one of the representative composite fracture theories (Erdogan and Sih 1963). In the case of mode I and mode II mixed loading, the polar coordinate components of the crack tip singular stress field can be expressed as:

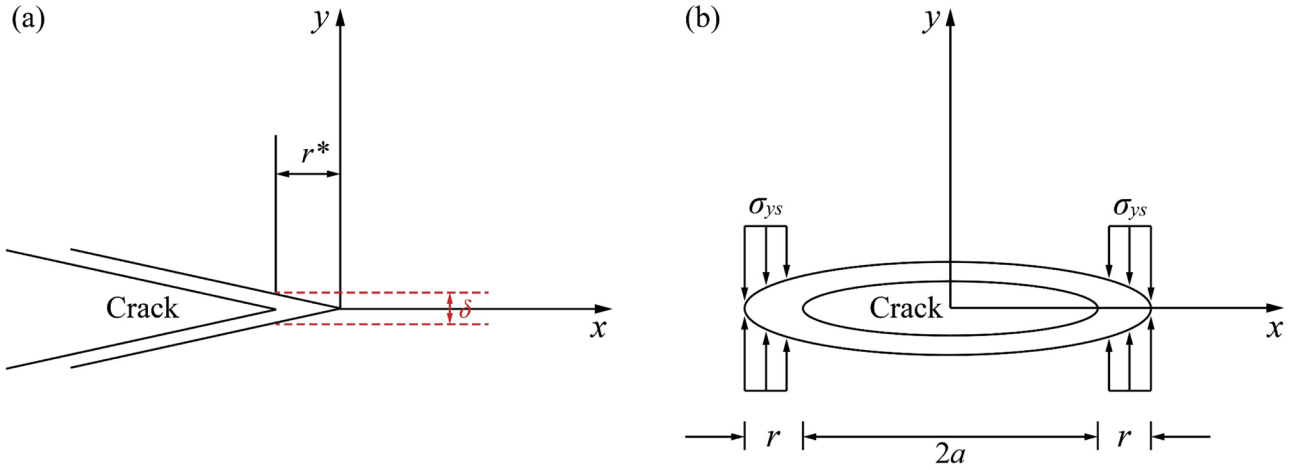

Fig. 5 (**a**) Definition of CTOD by Irwin method, (**b**) Dugdale model for the effective crack length

$$\begin{cases} \sigma_r = \frac{K_I}{2\sqrt{2\pi r}}(3-\cos\theta)cos\frac{\theta}{2} + \frac{K_{II}}{2\sqrt{2\pi r}}(3\cos\theta - 1)sin\frac{\theta}{2} \\ \sigma_\theta = \frac{K_I}{2\sqrt{2\pi r}}(1+\cos\theta)cos\frac{\theta}{2} - \frac{3K_{II}}{2\sqrt{2\pi r}}sin\theta cos\frac{\theta}{2} \\ \tau_\theta = \frac{K_I}{2\sqrt{2\pi r}}sin\theta cos\frac{\theta}{2} + \frac{K_{II}}{2\sqrt{2\pi r}}(3\cos - 1)cos\frac{\theta}{2} \end{cases} \tag{16}$$

where $\sigma_r, \sigma_\theta, \tau_r$ are the radial stress, hoop stress and shear stress near the crack tip, respectively; θ is the polar angle; r is the polar diameter. Therefore, the maximum hoop stress $\sigma_{\theta max}$ can be expressed as:

$$\sigma_{\theta\max} = \frac{1}{2\sqrt{2\pi r_0}}\cos\frac{\theta_0}{2}\left(K_I\cos\frac{\theta_0^2}{2} - 3K_{II}\sin\frac{\theta_0}{2}\cos\frac{\theta_0}{2}\right) \tag{17}$$

where θ_0 and r_0 are the critical values of polar angle and polar diameter, respectively. The fracture criterion based on maximum hoop stress can be expressed as Eq. (18):

$$\sigma_{\theta\max} \geq \sigma_{\theta\max C} \tag{18}$$

2.6 Critical strain energy density factor S_C

For mixed-mode cracks, another representative fracture criterion, is the strain energy density factor criterion which was proposed by Sih (1974) based on the local strain energy density field. The strain energy density factor fracture criterion should satisfy not only the minimum strain energy density factor reaching the critical value, but also the initiation of a crack along the direction of the smallest strain energy density factor. The expression of strain energy density factor S is:

$$S = a_{11}K_I^2 + 2a_{12}K_IK_{II} + a_{22}K_{II}^2 + a_{33}K_{III}^2 \tag{19}$$

where a_{11}, a_{12}, a_{22}, a_{33} are intermediate parameters, which can be obtained by Eq. (20):

$$\begin{cases} a_{11} = \frac{1}{16\pi E}((3-4v-\cos\theta)(1+\cos\theta)) \\ a_{12} = \frac{1}{8\pi E}sin\theta(\cos\theta - (1-2v)) \\ a_{22} = \frac{1}{16\pi E}(4(1-v)(1-\cos\theta) + (1+\cos\theta)(3\cos\theta - 1)) \\ a_{33} = \frac{1}{4\pi E} \end{cases} \tag{20}$$

Sih (1974) suggested that the crack propagation direction was along the minimum value of the strain energy density factor. The fracture criterion based on strain energy density factor can be expressed as Eq. (21):

$$S \geq S_C \tag{21}$$

3 Experimental investigation of soil fracturing

Section 2 focuses on fracture criterion and the significant of soil fracture mechanics parameters. In order to obtain these fracture mechanics parameters, researchers have performed numerous experimental investigations on soil fracturing. Among them are three-point bending tests, four-point bending tests, compact tension tests, ring tests, compression tests and other methods. Typical experimental methods for investigating soil fracturing behavior are summarized in Table 1.

Table 1 Summary of experimental studies on fracture parameters of various soil materials

Test method	Materials	Specimen type	Specimen dimensions	Fracture parameters	References
Three-point bending test	Clay mixed with 5% ordinary Portland cement	Single-edge notched beam	S×W×B: 250×100×100 mm, a: 50 mm	J_C	Chandler (1984)
	Frozen soil from Lanzhou		S×W×B: 300×100×100 mm, a: 40 mm	K_{IC}	Li and Yang (2000)
	Two mixtures of sand and kaolinite with different mass ratios: 75: 25, 50: 50		S×W×B: 90×20×20 mm, a: about 10 mm	CTOA, G_C	Hallett and Newson (2001)
	Sandy loam, clay loam, and cemented sand soil		S×W×B: 76×28×40 mm, a: 7 mm	K_{IC}	Aluko and Chandler (2006)
	Silty clay containing a small amount of gravels		S×W×B: 185×46×23 mm, a: 21~25 mm	K_{IC}	Wang et al. (2007b)
	Dry pure kaolinite		S×W×B: 140×34×31 mm, a: 12 mm	K_{IC}	Zhang et al. (2008)
	Bentonite and sand mix, Paddy soil		Unspecified	CTOA, J_C	Yoshida and Hallett (2008)
	Werribee clay		S×W×B: 140×30×30 mm, a: 10 mm	K_{IC}, G_C	Amarasiri et al. (2011)
	Unfired dry earth		S×W×B: 320×113×84 mm a: 44 mm	K_{IC}, CTOD	Lenci et al. (2012)
	Red clay		S×W×B: 200×50×25 mm, a: 1.0~4.0 mm; 320×80×40 mm, a: 1.0~7.0 mm	K_{IC}	Wang et al. (2016)
	Clay from Chongqing	Notched semi-circular bend specimen	S×W×B: 440×100×65 mm, a: Unspecified, Rout: 50 mm, a: 10~35 mm	K_{IC}	Wang et al. (2020)
Four-point bending test	Frozen soil from Lanzhou	Single-edge notched beam	S×W×B: 160×100×80 mm, a: about 50 mm	K_{IIC}	Li et al. (2000)
	Three mixtures of fine silica sand and kaolinite with different mass ratios: 20: 80, 40: 60 and Pure kaolinite (100%)		S×W×B: 140×25×25 mm, a: 12.5 mm	CTOA	Hallett and Newson (2005)
Three-point bending test and four-point bending test	Silty clay containing a small amount of gravels	Single-edge notched beam	S×W×B: 185×46×23 mm, a: 21~25 mm	K_{IC}, K_{IIC}	Wang et al. (2007a)

Table 1 (continued)

Test method	Materials	Specimen type	Specimen dimensions	Fracture parameters	References
Compact tension test	Overconsolidated cohesive soil	Compact tension specimen	S×W×B: 150×150×25 mm; a: 60 mm	G_C	Lee et al. (1988)
	Intact Saint-Alban clayey soil		S×W×B: 130×130×54 mm; a: 40, 50, 70 mm	K_{IC}, G_C	Ayad et al. (1997)
	Frozen base and subbase soils in pavement		S×W×B: 130×130×54 mm, a: 40, 55, 70 mm	K_{IC}	Konrad and Cummings (2001)
	Barcelona silty clay		S×W×B: 60×45×25 mm, 120×90×50 mm, a: 10, 15, 20 mm (20, 30, 40 mm)	K_{IC}, G_C	Lakshmikantha et al. (2008, 2012), Prat et al. (2008)
Ring test	Two residual soils from Kentucky (CL and ML soils)	Compact circular ring specimen	R_{out}×R_{in}×B: 50×6.25×12.5 mm	K_{IC}, GC, J_C	Harison et al. (1994)
	Werribee clay and kaolin clay	Double circular ring	R_{out}×R_{in}×B: 104×33×10 mm, 104×55×10 mm	J_C, G_C	Costa and Kodikara (2012), Costa et al. (2013b, 2016)
Indirect tension test	Three mixtures of fine silica sand and kaolinite with different mass ratios: 1000: 250, 1000: 667, 1000: 1500	Centre crack cylinder	D: 27.6, 52.0, 77.5, 102.3 mm; a: 5.244, 9.880, 19.437 mm	K_{IC}	Hallett et al. (1995)
Tri-axial compression test	Soft pyroclastic ash loam	Centre crack cylinder	D×H: 70×100 mm, 80×100 mm, 90×100 mm, a: 10 mm	K_{IC}	Nishimura and Shimizu (2004)
Uniaxial unconfined compression fracture test	Shenyang-specific silty clay	Compact compression specimen	S×W×H: 90×90×200 mm, a: 50–55 mm	K_{IC}, K_{IIC}	Liu and Liu (2011)

K_{IC}: Mode-I fracture toughness; K_{IIC}: Mode-II fracture toughness; G_C: Critical energy release rate; J_C: *J* integral; *CTOA*: Crack Tip Opening Angle; *CTOD*: Crack Tip Opening Displacement; *S*: Effective length of specimen; *W*: Width of specimen; *B*: Thickness of specimen; *D*: Diameter of specimen; *H*: Height of specimen; *a*: Initial length of crack; R_{in}: Inner radius of specimen; R_{out}: outer radius of specimen

3.1 Three-point bending test

Following ASTM International (ASTM E399-20 2020), the standard proportions and tolerances of the single-edge notched beam (SENB) is shown in Fig. 6, which can be used as the standard specimen to determine the plane strain fracture toughness of the material including soil, metal, concrete, ceramics, and rock (Wang et al. 2007a). However, this standard is more suitable for brittle materials, but the soil is not a completely brittle material. For a given state of a particular soil, there is no specific standard method in measuring soil fracture toughness up to now. It is recommended to measure the soil fracture toughness according to the method provided by the ASTM International (ASTM E399-20 2020). In order to ensure the linear elastic behavior and minimize the size effect of the specimen, the following criteria are used on the sample size and initial crack length:

$$\begin{cases} (W-a) \geq 2.5\left(\frac{K_I}{\sigma_{ys}}\right)^2 \\ a \geq 2.5\left(\frac{K_I}{\sigma_{ys}}\right)^2 \\ B \geq 2.5\left(\frac{K_I}{\sigma_{ys}}\right)^2 \end{cases} \tag{22}$$

where W is the width of specimen, B is the thickness of specimen. Sture et al. (1999) proposed that when the a/W of cemented sand is in the range of 0.2–0.55, the stress intensity factor K of the three-point bending specimen can be calculated according to the following Eq. (23):

$$K_I = \frac{PS}{BW^{3/2}} f_1\left(\frac{a}{W}\right) \tag{23}$$

where S is the effective length of specimen, P is the concentrated load applied on the specimen, f_1 is a function of a/W, which can be express as:

$$f_1\left(\frac{a}{W}\right) = \frac{3\left(\frac{a}{W}\right)^{1/2}\left(1.99 - \left(\frac{a}{W}\right)\left(1-\frac{a}{W}\right)\left(2.15 - 3.93\frac{a}{W} + 2.7\frac{a^2}{W^2}\right)\right)}{2\left(1+\frac{2a}{W}\right)\left(1-\frac{a}{W}\right)^{3/2}} \tag{24}$$

A number of researchers have used the standard three-point bending test to successfully determine the fracture toughness or crack tip opening displacement (*CTOD*) of soil specimens (Li and Yang 2000; Aluko and Chandler 2006; Zhang et al. 2008; Lenci et al. 2012). For example, Lenci et al. (2012) investigated the rupture behavior of the unfired dry earth by the testing apparatus shown in Fig. 7a. The three-point bending test was carried out under monotonic and cyclic loading and the related force–displacement diagrams were theoretically interpreted to characterize the fracture parameters (K_{IC} and *CTOD*) of the soil material.

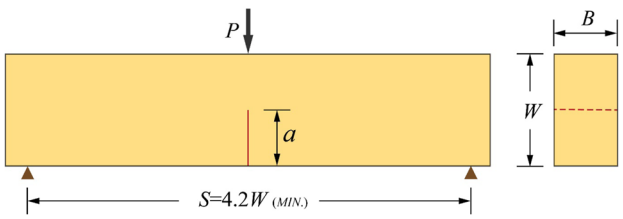

Fig. 6 Standard single edge cracked beam (ASTM E399-20, 2020)

In the standard three-point bending test, the weight of samples will have an effect on the accuracy of testing results, even if the specimen may not rupture failure under the action of its weight. Compared with the concentrated load, the self-weight of the specimen is not an insignificant quantity that can be ignored. Furthermore, the bending moment generated by the specimen self-weight at the crack face, changes continuously with the deformation of the specimen during the bending test.

In order to minimize or remove the impact of the specimen self-weight on the test results, researchers have utilized a series of improved three-point bending test apparatuses in their studies. Two retractable supports were installed by Chandler (1984) on both sides of the initial crack at the specimen bottom, which can symmetrically balance the specimen self-weight. The results show that the tested soil behaves like a tough metal as the internal crack growth resistance increases remarkable with crack growth. As illustrated in Fig. 7b, Hallett and Newson (2001) installed two glass slides on the bottom of the specimen that can rotate around the rollers. Weights were placed on both ends of the glass slides to balance against the soil specimen self-weight. The same balancing principle is used in Yoshida and Hallett (2008) and Amarasiri et al. (2011). Wang et al. (2007a, 2007b, 2016) rotated the bottom side of the original specimen by 90° to make the direction of the load P perpendicular to the weight direction of the soil specimen (shown in Fig. 7c), which not only prevented the soil specimen from fracturing solely under its self-weight, but also makes the variation curve easy to obtain after the peak load. Actually, the influence of the specimen self-weight cannot be completely eliminated, because the specimen is a soil beam with a specific thickness.

In order to minimize the disturbance that crack prefabrication and sample transfer can impose on a sample due to the low strength of the soil during test preparation, Wang et al. (2020) proposed the use of notched semi-circular bend specimens (NSCB) for three-point bending tests on account of their small dimensions and ease of testing as shown in Fig. 7d. According to LEFM, the initial crack starts to fracture from the crack tip under the action of concentrated load P. The K_{IC} value of the NSCB specimen can be determined by the following Eqs. (25) and (26):

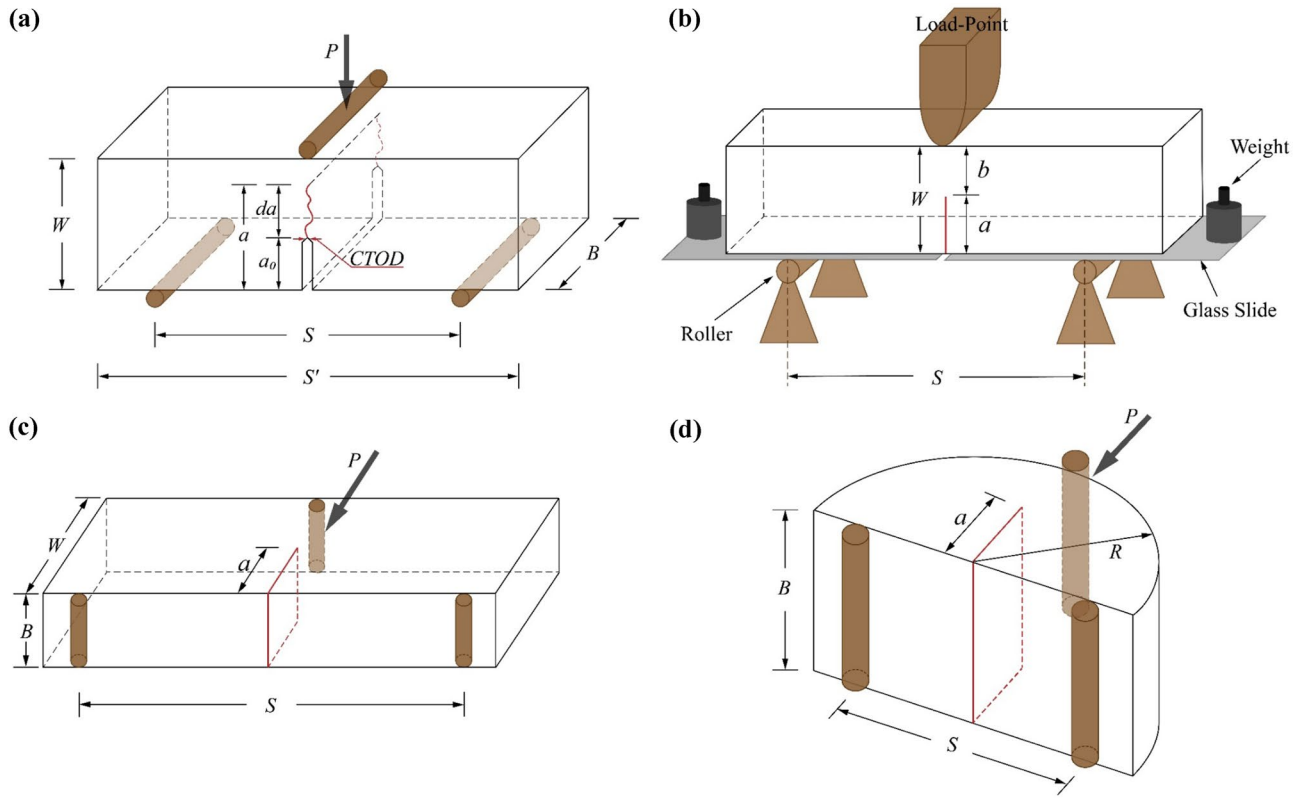

Fig. 7 Four geometrical configurations of the three-point bending test (Hallett and Newson 2001; Wang et al. 2007a, 2020; Lenci et al. 2012)

$$K_{IC} = Y\frac{P_{max}\sqrt{\pi a}}{2BR}(a/R \geq 0.2) \tag{25}$$

$$Y = -1.297 + 9.516\frac{S}{2R} - \left(0.47 + 16.457\frac{S}{2R}\right)\frac{a}{R} + \left(1.071 + 34.401\frac{S}{2R}\right)\left(\frac{a}{R}\right)^2 \tag{26}$$

where P_{max} is the critical value of concentrated load, Y is the nondimensionalize stress intensity factor (SIF) corresponding to specimen geometry, R is the radius of semicircular specimen.

3.2 Four-point bending test

The three-point bending test is mainly used to determine fracture toughness in mode I cracking, but the actual cracking mode of the soil is usually more complicated. It could be mode I, mode II or mixed mode. Therefore, it is not enough to solely study mode I cracking of soil. In addition to the three-point bending test, the four-point bending test is an important method for determining the fracture toughness in mode II cracking and the stress intensity factors of mixed mode I-II cracking during the fracture propagation of soil specimens. Wang et al. (2007a) proposed an improved four-point asymmetric bending test configuration with horizontal concentrated load, as presented in Fig. 8a. The shear force and bending moment that act on the crack plane, can be obtained based on the force and moment equilibrium theories drawn from in engineering mechanics, which can be expressed as Eq. (27):

$$\begin{cases} Q = \frac{L_1 - L_2}{L_1 + L_2}P \\ M = \left(L_2 + c\right)\frac{L_1}{L_1 + L_2}P - \left(L_1 + c\right)\frac{L_2}{L_1 + L_2}P \end{cases} \tag{27}$$

where Q and M are the shearing and force bending moment on crack plane; P is concentrated load applied on the specimen; L_1 and L_2 the horizontal distance from the application point of concentrated load P to fulcrums A (or D) and B (or C), respectively; c is the horizontal distance from the application point of concentrated load P to the initiate crack. While the crack length a is 0.25 ~ 0.75 times as long as the specimen width W, the stress intensity factor K of the four-point bending specimen is calculated according to the following equation (Lin and Xue 1985):

$$\begin{cases} K_I = \frac{M}{BW^{3/2}}f_2\left(\frac{a}{W}\right) \\ K_{II} = \frac{Q}{BW^{3/2}}f_3\left(\frac{a}{W}\right) \end{cases} \quad (a = 0.25 \sim 0.75W) \tag{28}$$

where f_2 and f_3 are functions of a/W, which can be expressed as:

$$\begin{cases} f_2\left(\frac{a}{W}\right) = \frac{6\left(\frac{a}{W}\right)^{1/2}\left(1.99-\left(\frac{a}{W}\right)\left(1-\frac{a}{W}\right)\left(2.15-3.93\frac{a}{W}+2.7\frac{a^2}{W^2}\right)\right)}{\left(1+\frac{2a}{W}\right)\left(1-\frac{a}{W}\right)^{3/2}} \\ f_3\left(\frac{a}{W}\right) = \left(1.442-5.08\left(\frac{a}{W}-0.507\right)^2\right)sec\frac{\pi a}{2W}\sqrt{\sin\frac{\pi a}{2W}} \end{cases} \tag{29}$$

If c is equal to zero, according to Eq. (27), the bending moment acting on the crack plane is also equal to zero. This means that the type of crack is a mode II crack. In this condition, the stress intensity factor for the mode II crack is obtained by using Eq. (28). When the concentrated load P is the critical load for crack instability propagation, the stress intensity factor is the K_{IIC} of the soil specimen. Li et al. (2000) used the same four-point bending device to measure the K_{IIC} of the soil. The behavior of the interface between the soil and concrete, K_{IIC} can be expressed as:

$$K_{IIC} = \frac{P_{max}}{3BW^{1/2}}\left(1.442-5.08\left(\frac{a}{W}-0.567\right)^2\right)\sec\frac{\pi a}{2W}\sqrt{\sin\frac{\pi a}{2W}} \tag{30}$$

If c is unequal to zero, on the basis of Eq. (27), the shearing force and bending moment acting on the crack plane are also unequal to zero, which means that the type of crack is mixed mode I-II crack. When the concentrated load P is the critical load for fracturing failure, the stress intensity factors are the K_{IC} and K_{IIC} of the soil specimen.

Hallett and Newson (2005) collected data on load transmission, specimen bending, crack propagation and crack-mouth opening to evaluate the crack tip opening angle (CTOA) using a modified four-point bending test device (shown in Fig. 8b). In the experiment, a new method that is based EPFM was used to describe the formation of cracks in a plastic soil by the CTOA. As illustrated in Fig. 8c, crack evolution in wet soil during the flexure test can be divided into three stages. In the first stage (crack opening), once the yield point is exceeded, the crack will open such that the plastic strain energy will accumulate at the crack tip. During the second stage (crack initiation), the crack begins to propagate and the plastic strain energy be released with corresponding drop in the force applied. In the third stage (stable ductile crack growth), once the ductile crack propagation becomes stable, steady-state conditions will occur.

3.3 Compact tension test

Following ASTM International (ASTM E399-20 2020), the compact tension (CT) specimen (the standard configurations are shown in Fig. 9) can be used as another standard specimen to determine the plane strain fracture toughness of the material. This is composed of a single edge notched and fatigue pre-cracked plate under tensile load. The requirements concerning sample size and initial crack length have been mentioned in Eq. (22). The stress intensity factor K of the compact tension specimen is calculated based on the following Eq. (31):

$$K = \frac{P}{BW^{1/2}}f_4\left(\frac{a}{W}\right) \tag{31}$$

where f_4 is functions of a/W, which can be express as:

$$f_4\left(\frac{a}{W}\right) = \frac{\left(2+\frac{a}{W}\right)\left(0.886+4.64\frac{a}{W}-13.32\left(\frac{a}{W}\right)^2+14.72\left(\frac{a}{W}\right)^3-5.6\left(\frac{a}{W}\right)^4\right)}{\left(1-\frac{a}{W}\right)^{3/2}} \tag{32}$$

Konrad and Cummings (2001) used the fracture mechanics test procedure recommended by the ASTM Standard E399-83 to determine the fracture toughness of sand layer-base and crushed stone layer-base. The value of K_{IC} can be calculated by using Eq. (33) (ASTM E399-83, 1983):

$$K_{IC} = \frac{P_{max}}{Ba^{1/2}}f_5\left(\frac{a}{W}\right) \tag{33}$$

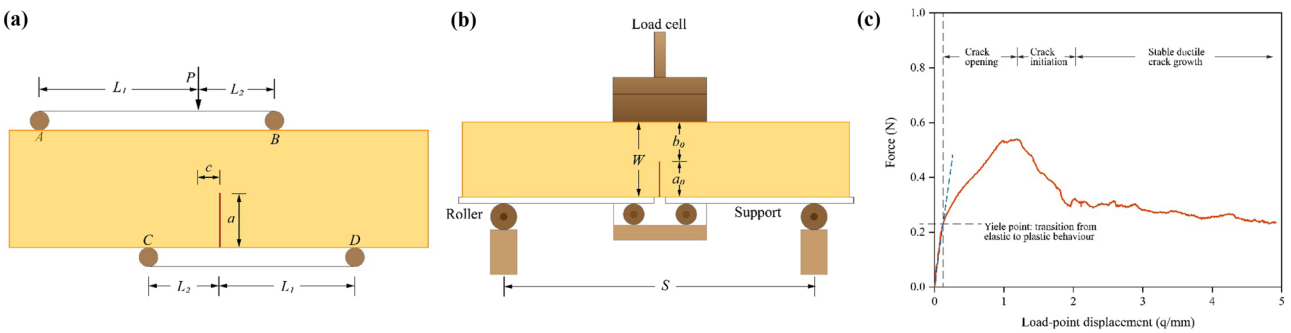

Fig. 8 Two geometrical configurations of four-point bending test and the stages of crack evolution in wet soil during the flexure test. (Hallett and Newson 2005; Wang et al. 2007a)

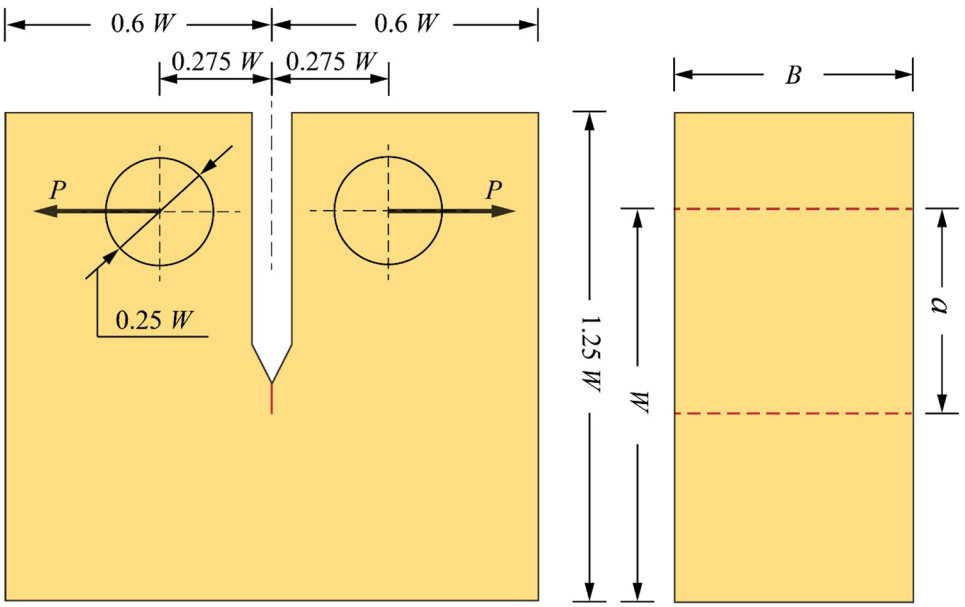

Fig. 9 Compact tension specimen with standard proportions (ASTM E399-20 2020)

where f_5 is functions of a/W, which can be expressed as:

$$f_5\left(\frac{a}{W}\right) = 30.96\left(\frac{a}{W}\right) - 195.8\left(\frac{a}{W}\right)^2 + 730.6\left(\frac{a}{W}\right)^3 - 1186.3\left(\frac{a}{W}\right)^4 + 754.6\left(\frac{a}{W}\right)^5 \quad (34)$$

In order to study the relationship between tensile strength and fracture toughness of soil and the size effect of soil cracking, Lakshmikantha et al. (2008, 2012) used a direct tensile strength equipment and a CT-test equipment to obtain the two parameters. The schematic diagram of CT-test equipment is shown in Fig. 10. For convenience of comparison, two methods were used for processing fracture toughness data obtainable through Eq. (31) and Eq. (33). Prat et al. (2008) used the same method to determine the fracture toughness and tensile strength of soil specimens with different water contents, and formulated a numerical model to study the initiation and propagation of soil desiccation cracks based on soil mechanics and fracture mechanics.

In addition to fracture toughness and stress intensity factors, the critical energy release rate can also be obtained using the compact tension (CT) test (Lee et al. 1988; Ayad et al. 1997). Ayad et al. (1997) suggested that the critical energy release rate due to crack growth corresponds to the difference in value between the rate of work done by external loading and the rate of increase in strain energy of the specimen. The definition of specimen compliance (λ) is as follows:

$$\lambda = \frac{u_c}{F_c} \quad (35)$$

where F_c is the fracture load, u_c is the load point displacement. The critical energy release rate can be expressed as:

$$G_C = \frac{1}{2B}F_c^2\frac{d\lambda}{da} \quad (36)$$

3.4 Ring test

Due to plastic behavior near the crack tip, LEFM has limitations in analyzing the cracking of some non-brittle materials, especially, the desiccation crack of wet or slurried soils (Amarasiri and Kodikara 2011; Costa and Kodikara 2012). The size of the crack must be much larger than the size of the plastic zone, so that the crack body can be seen as a whole with approximately elastic manner (Janssen et al. 2004). Cracking problems that do not meet these required extreme conditions have to be studied using EPFM theory. Compared with LEFM, EPFM is a relatively complicated method of analyzing soil cracking. It has not been well developed so far. As discussed in Subsections 2.3 and 2.4, the J integral and CTOD are also two significant EPFM fracture parameters in the study of soil cracking. When the soil transforms from a highly plastic state to an elastic or quasi-brittle state due to desiccation, the J integral become a general fracture parameter for the soil. The ring test is mainly used to obtain the value of J integral, which has been widely used to evaluate the stress development, the strength changes and the cracking behavior of fiber reinforced concrete or polymer-modified asphalt concrete (Mindess et al. 1977; Velazco et al. 1980; Bhurke et al. 1997; Kuai et al. 2009).

Harison et al. (1994) used the ring test to determine the fracture toughness and the critical J integral of 132 compacted samples of two fine grained soils and compared the fracture toughness values measured by the bending test and the ring test. The configuration of ring test and crack-tip

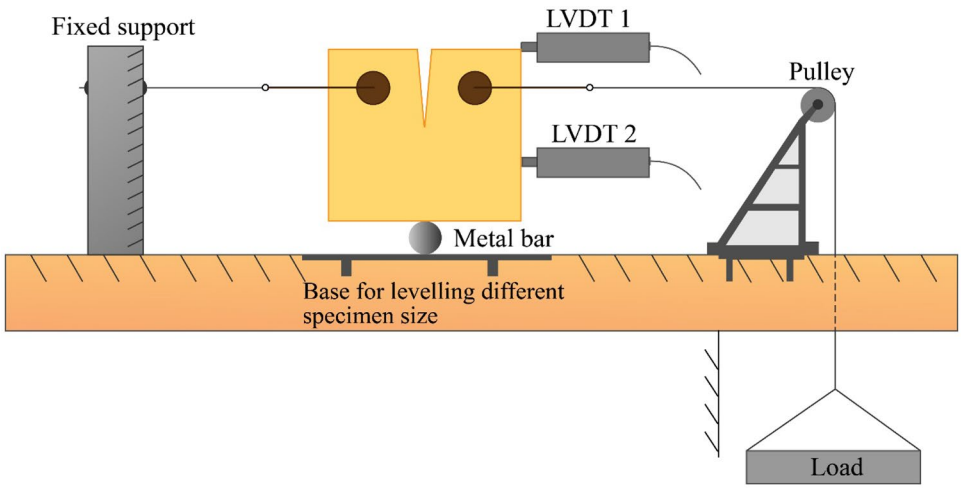

Fig. 10 Schematic diagram of CT-test equipment (Lakshmikantha et al. 2008)

model are shown in Fig. 11a. The expression of J integral form is transformed into the integral area of the load and load point displacement curve (Rice et al. 1973):

$$J = \frac{1}{B}\int_0^{\delta}\left(-\frac{\partial P}{\partial a}\right)d\delta \tag{37}$$

Rice et al. (1973) suggested that the total load point displacement of the cracked specimen should be separated into two parts, namely, the measurable displacement without the initial crack $\delta_{nocrack}$ and the displacement caused by the introduction of initial crack δ_{crack}. If the integrated area of the P-load point displacement curve measured when the sample is free of cracks is A_{nc}, and the integrated area measured after the cracks are introduced is A_c, the J integral described by Eq. (37) can be written as following:

$$\begin{aligned} J &= \frac{f'(a)}{f(a)}\frac{1}{B}\int_0^{\delta_{crack}} P d\delta_{crack} \\ &= \frac{f'(a)}{f(a)}\frac{1}{B}\left(A_c - A_{\mathrm{nc}}\right) \end{aligned} \tag{38}$$

where $f(a)$ is the function determined by the ratio of δ_{crack} to the load P, $f'(a)$ is the derivative of $f(a)$.

Costa and Kodikara (2012) proposed an innovative ring test to determine fracture properties (J integral) during the drying process of a clayey soil. The schematic diagram of slurry specimen is shown in Fig. 11b. This is the first time that fracture mechanics is applied to study the drying of slurry specimens. As presented in Fig. 11b, the J integral can be expressed as the sum of several line integrals based on the basic principles of fracture mechanics (Luo et al. 2003), is defined as:

$$J = J_{V1} + J_{H2} + J_{V2} + J_{H1} \tag{39}$$

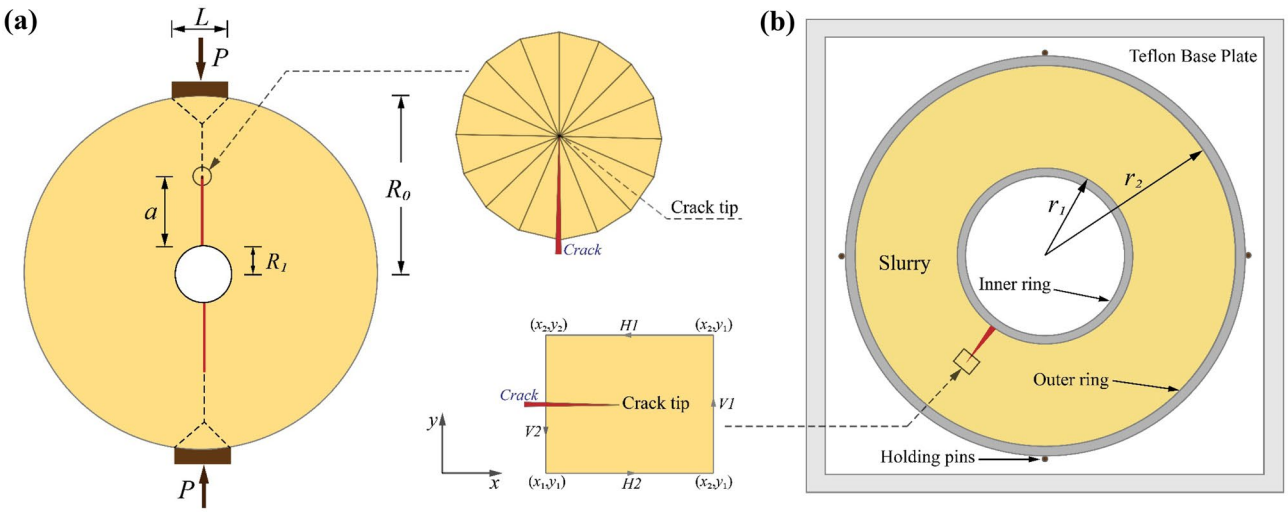

Fig. 11 Two configuration of ring test (Harison et al. 1994; Costa and Kodikara 2012)

where

$$\begin{cases} cJ_{V1} = \int_{y_1}^{y_2} Wdy - \left(\sigma_{xx}\frac{\partial u_x}{\partial x} + \sigma_{xy}\frac{\partial u_y}{\partial x}\right)dy \\ J_{V2} = \int_{y_2}^{y_1} Wdy - \left(\sigma_{xx}\frac{\partial u_x}{\partial x} + \sigma_{xy}\frac{\partial u_y}{\partial x}\right)dy \\ J_{H1} = -\int_{x_2}^{x_1}\left(\sigma_{yy}\frac{\partial u_x}{\partial x} + \sigma_{yx}\frac{\partial u_x}{\partial x}\right)dx \\ J_{H2} = -\int_{x_1}^{x_2}\left(\sigma_{yy}\frac{\partial u_y}{\partial x} + \sigma_{yx}\frac{\partial u_x}{\partial x}\right)dx \end{cases} \quad (40)$$

where V_1, V_2, H_1 and H_2 are the four paths of four line integrals, respectively; u_x, u_y, *and* σ_{yy} are the displacements and stress in x and y directions, respectively.

It is worth mentioning that particle image velocimetry (PIV) analysis is used to obtain the strain and stress of the slurry specimen surface which can be later used to calculate the J integral. Then, according to the same method, Costa et al. (2013b, 2016) later not only calculated the J integral of Churchill clay and kaolin clay by using the new ring test, but also got the J integral of mud specimens and compacted soil specimens with the corresponding linear shrinkage coefficient. In addition, the independence of the J integral calculation path and the relationship between the J integral and the water content were also analyzed.

3.5 Other methods

In addition to the four test methods discussed above, there are some indirect methods exemplified by the compression test that can be used to determine the soil fracture parameters (Hallett et al. 1995; Nishimura and Shimizu 2004; Liu and Liu 2011). Centre cracked cylinder specimens with initial tension cracks were set in advance and made of three mixtures of silica sand and kaolinite. They were tested to determine fracture toughness by an indirect tension test (Hallett et al. 1995). The configuration of indirect tension test is shown in Fig. 12a. Hallett et al. (1995) found that the plastic zone (as presented in Fig. 12a) at the pre-existing crack tip was significant due to the crack propagation. This could explain the additional energy dissipation during crack development. In general, the relationship between the crack direction and the stress affects the stress intensity and failure mode of the crack tip. In the test, the failure mode of the pre-existing crack is of mode I type. Therefore, the fracture toughness is evaluated as follows:

$$K_{IC}=Y\sigma_f a^{1/2} \quad (41)$$

where

$$\begin{cases} \sigma_f = \frac{F_c}{\pi R_0 l} \\ Y\left(\frac{a}{2R_0}\right) = 1 + \frac{3}{2}\left(\frac{a}{R_0}\right)^2 + \frac{3}{4}\left(\frac{a}{R_0}\right)^6 + \frac{3}{64}\left(\frac{a}{R_0}\right)^8 \end{cases} \quad (42)$$

Where σ_f is the failure stress of the disc, R_0 is radius of the disc, l is length of the disc, Y is the specimen geometry stress intensity factor.

Liu and Liu (2011) used soil specimens containing wing cracks with different inclination angles to perform uniaxial unconfined compression fracture experiments. The specimen dimension and the location of external load are illustrated in Fig. 12b. The model of compression and shear fracture of wing cracks is also presented in Fig. 12b. It is noteworthy that the failure mode of the compression specimen is the mixed mode I-II cracking type. Therefore, the fracture toughness of the wing crack specimens including two failure modes (mode I and mode II), can be expressed as:

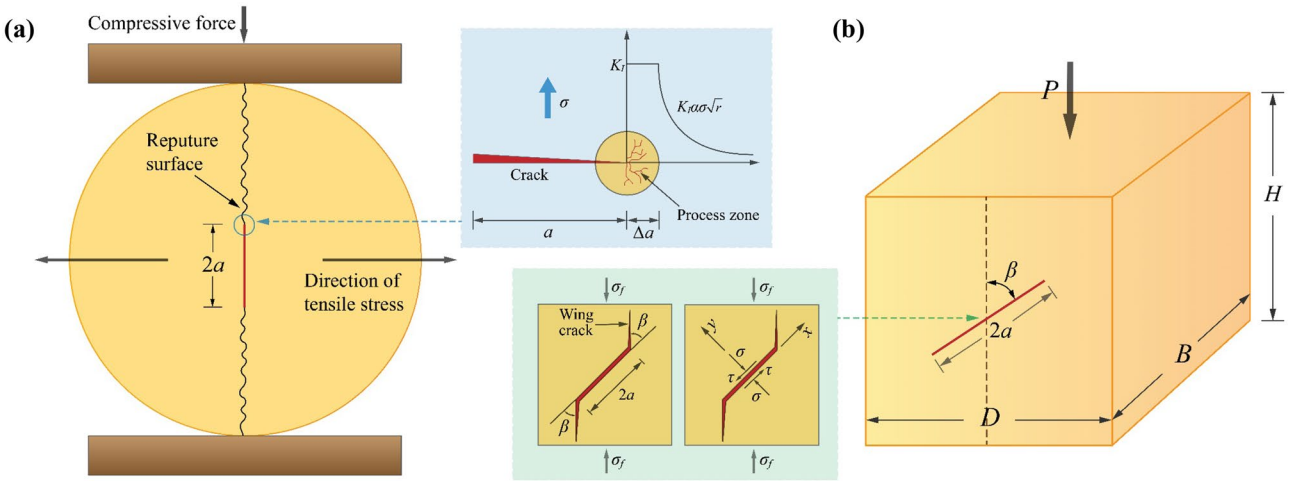

Fig. 12 Two configurations of compression test (Hallett et al. 1995; Liu and Liu 2011)

$$\begin{cases} K_{IC} = \frac{1}{2}\sigma_f(1+\cos 2\beta)\sqrt{\pi a} \\ \quad = \sigma_f\sqrt{\pi a}\sin^2\beta \\ K_{IIC} = \left(-\frac{1}{2}\sigma_f \sin 2\beta\right)\sqrt{\pi a} \\ \quad = \sigma_f\sqrt{\pi a}sin\beta cos\beta \end{cases} \tag{43}$$

where β is the angle between the pre-existing crack and the failure stress σ_f which also called the crack angle.

This section introduces the five main test methods used to determine soil fracture parameters. It is obvious that each method has its advantages and limitations. Although the three-point and the four-point bending tests are very convenient, the self-weight of the specimen in both tests affects the accuracy of the fracture parameters. Although some researchers have improved the test device based on different principles, they still cannot completely overcome this problem. Compact tension test is also one of the important methods to measure soil fracture parameters. Although it can remove the influence of its self-weight on the test results, it is likely that failure of the specimen loading point will precede the comprehensive failure of the specimen because of the low tensile strength of the soil. The ring test is mainly used to obtain the value of J integral based on EPFM, which is the first time that fracture mechanics is applied to the study of the drying process of slurry specimens. This test method has been widely applied to evaluate stress development. However, the procedures of ring test are too cumbersome for frequent use in the testing of soil cracking. Consequently, the ring test is rarely used. The compression test can also be used to measure soil fracture toughness, it is mainly used to test soils of the relatively high strength regime. Pre-existing cracks and external loading pattens of the compression specimens affect the accuracy of fracture parameters of soil samples, especially when the samples are of lower strength.

4 Factors that affect soil fracturing parameters

The fracture process of soil is complicated, because soils are composites of various grains of diverse minerals that interact at different levels of bond strength. External factors, including test protocols affect soil fracture as setting. Thus, the factors influencing soil fracture parameters can be categorized into two major groups, including soil intrinsic properties and test-related factors.

4.1 Soil intrinsic properties

Soil is a multi-phase material that consists of soil particles (solid phase), water (liquid phase) and air (gaseous phase). The existence of different phases leads to the inhomogeneity, a characteristic which also reflects other properties, including water content (w), dry density (p), clay content and so forth. Table 2 is a summary of research that has been performed on the effects of soil intrinsic properties on fracturing parameters.

4.1.1 Water content

Soil characteristics, especially for fine grained soils change with water content (Haynes and Swift 1990). Water does not exist in soil merely as another physical component but participates in complex physical–chemical interactions with soil particles. These interactions are partial determinants of the engineering properties of the soil. Changes in soil water content inevitably influence the ability of soil to resist fracturing and this is reflected in the value of soil fracture toughness (Wang et al. 2007a).

Figure 13 shows how water content influences the fracture toughness of soils. In addition to the results obtained by Wang et al. (2007a), other test results indicate that the value of fracture toughness decreases with increase in water content. As the compacted specimen is in an unsaturated state, the change of water content may result in the change of bond water thickness among soil particles. Meanwhile, the interaction force among soil particles and suction potential in the soil will have been changed (Amarasiri et al. 2011; Lakshmikantha et al. 2008, 2012; Wang et al. 2007a, 2007b, 2020).

4.1.2 Dry density

Dry density of a soil can be defined as the ratio of mass of solids to the total volume of a soil. This parameter is thus determined by the proportions of the solid phase soil particles and pores in the soil. When the relative density of soil particles is fixed, soil dry density reflects the total amount of pores in the soil, itself a reflection of the degree of compaction of the soil. Therefore, a change in dry density is usually a change in soil strength. These same factors affect fracture behavior of soil. Considering that most threats of soil fracture in geotechnical works involve compacted soils, the dry density is thus an important parameter in soil fracture (Wang et al. 2007b; Demagistri et al. 2018).

Figure 14 illustrates the dependence of fracture toughness on dry density. Wang et al. (2007a, 2007b, 2020) concluded that the value of fracture toughness increases linearly as specimen dry density increases. This is consistent with the findings on the desiccation cracking of compacted soil with different dry densities (Albrecht and Benson 2001). Volumetric shrinkage strain decreases with increasing compaction effort. Samples with the largest

Table 2 Influence of soil intrinsic properties on fracture parameters

Soil intrinsic properties	Variation component and range	Fracture parameters	Research results	References
Water content	15.4%, 16.6%, 17.4%, 18.3%, 19.0%, 19.6%	K_{IC}	There exists an optimal water content between K_{IC} and specimen water content	Wang et al. (2007a)
	16.3%, 17.3%, 18.4%, 19.3%	K_{IC}	K_{IC} value decreases as specimen water content increases	Wang et al. (2007b)
	16%, 18%, 19%, 21%	K_{IC}, G_C	K_{IC} value decreases exponentially as specimen water content increases	Lakshmikantha et al. (2008)
	17.6%, 21.3%, 30.0%, 38.3%	K_{IC}, G_C	K_{IC} and G_C value decreases exponentially as specimen water content increases	Amarasiri et al. (2011)
	16%, 17%, 18%, 19%, 20%, 21%	K_{IC}, G_C	K_{IC} and G_C value decreases exponentially as specimen water content increases	Lakshmikantha et al. (2012)
	14.6%, 16.6%, 18.6%, 20.6%	K_{IC}	K_{IC} value decreases lineally as specimen water content increases	Wang et al. (2020)
Dry density	1.68, 1.70, 1.72, 1.74, 1.76 g/cm^3	K_{IC}	K_{IC} value increases linearly as specimen dry density increases	Wang et al. (2007a)
	1.60, 1.65, 1.72, 1.74 g/cm^3		K_{IC} value increases as specimen dry density increases	Wang et al. (2007b)
	1.62, 1.64, 1.66, 1.68, 1.70 g/cm^3		K_{IC} value increases linearly as specimen dry density increases	Wang et al. (2020)
Clay content	Two mixtures of sand and kaolinite with different mass ratios: 75: 25, 50: 50	COA, G_C	The specimen with a ratio of sand to kaolinite of 75:25 need more energy to drive crack propagation, as compared with 50:50	Hallett and Newson (2001)
	Three mixtures of fine silica sand and kaolinite with different mass ratios: 20: 80, 40: 60 and Pure kaolinite (100%)	CTOA	Changing the ratio of silica sand: kaolinite clay slightly from 0:100 to 20:80 caused the *CTOA* almost to halve, from 0.230 mm^{-1} to 0.136 mm^{-1}	Hallett and Newson (2005)
Salinity	Pure kaolinite and saline pure kaolinite (0.5 M NaCl)	CTOA	Salinity (0.5 M NaCl) reduces the *CTOA* of pure kaolinite from 0.23 mm^{-1} to 0.17 mm^{-1}	Hallett and Newso. (2005)
Polygalacturonic acid (PGA)	Pure kaolinite was mixed with 0, 1.2, 2.4, 4.9 or 12.2 g PGA kg^{-1}	K_{IC}	K_{IC} increased exponentially with added PGA, with washing increasing this trend	Zhang et al. (2008)

K Mode-I fracture toughness; *K* Mode-II fracture toughness; G_C Critical energy release rate *CTOA*: crack tip opening angle

volumetric shrinkage strains typically contained the largest number of cracks. For the compacted soil with a certain water content, the bulk density and clay content increase with the increase of dry density. At the same time, as the dry density increases, the distance between the soil particles gradually decreases and the contact areas among soil particles increase, resulting in an increase in friction among the soil particles. Therefore, the higher the dry density of the specimen is, the more difficult the initial crack propagation will be.

In addition to water content and dry density, some researchers have also studied the influence of clay, salinity and admixture content on soil fracture parameters (Hallett and Newson 2001, 2005; Zhang et al. 2008). The greater the proportion of sand in a soil mix, the smaller the crack tip opening angle (CTOA) will be as a reflection of the higher energy requirement for crack extension. To be specific, the specimens with ratios of sand to kaolinite of 75:25 and 50:50 were tested for bending. CTOA values of 0.19 mm^{-1} to 0.24 mm^{-1} were obtained, which indicate that more strain is needed for crack propagation (Hallett and Newson 2001). Furthermore, changing the ratio of silica sand to kaolinitic clay slightly from 0:100 to 20:80 reduces the CTOA by about 50%, from 0.230 mm^{-1} to 0.136 mm^{-1} (Hallett and Newson 2005).

Hallett and Newson. (2005) added a salt (0.5 M NaCl) to pure kaolinite in their tests and found that CTOA changed from 0.23 mm^{-1} to 0.17 mm^{-1}. This means that

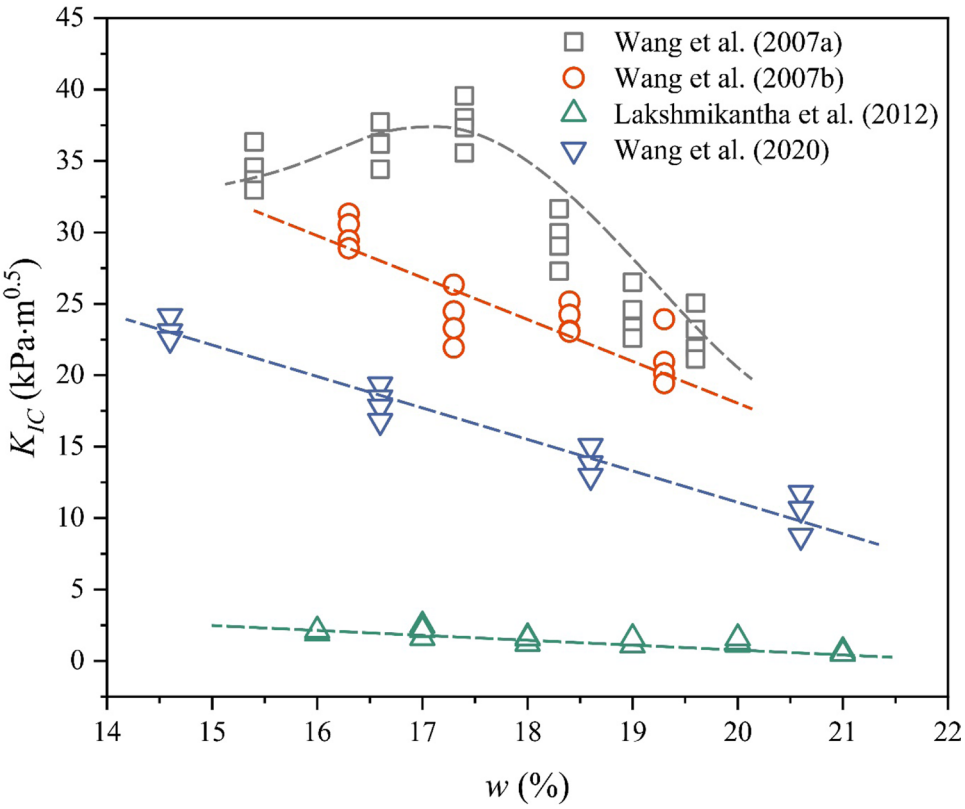

Fig. 13 The dependence of fracture toughness on water content

the soil saline samples require more energy for crack development when compared with non-saline samples. Increase in salinity produces a reduction in soil surface crack ratio (Zhang et al. 2019). In other words, the distribution density of the crack networks on the soil surface is reduced with increased salinity, but more centralized (DeCarlo and Shokri 2014; Shokri et al. 2015; Zhang et al. 2016, 2019).

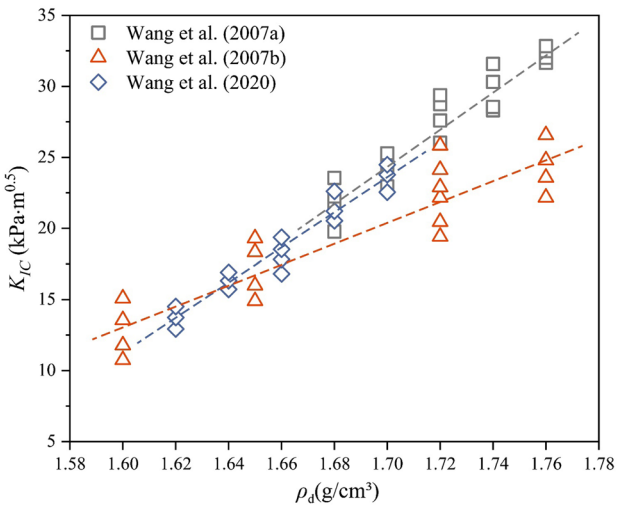

Fig. 14 The dependence of fracture toughness on dry density

In order to quantify the effect of root exudates (polygalacturonic acid (PGA)) on the interparticle bond energy and fracture toughness of clay, Zhang et al. (2008) used pure kaolinite mixed with different PGA content to form test samples. Half of the test samples were washed repeatedly to remove unbound PGA and evaluate the persistence of its effects. The results show that soil fracture toughness increases exponentially with added PGA and that soil washing increases this trend. This use of fracture mechanics in analysis enables assessment of the stability of the rhizosphere and has implications in soil erosion and agriculture.

4.2 Test-related factors

The determination of soil fracture parameters is strongly dependent on test sample preparations and test conditions. Among these parameters are the ratio of initial crack length to specimen width (a/W), environmental temperature (T), loading rate (P_L), specimen thickness and so on. Many investigations have focused on the influence of these tested-related factors on the soil fracture behavior. Table 3 is a summary of how the test-related factors influence the soil fracture parameters.

4.2.1 The ratio of initial crack length to specimen width

Fracture toughness is the resistance of soil to fracture. It is assigned to the state of the material, and has nothing to

do with the change of a/W. Therefore, when the value of fracture toughness changes with the initial crack length, it should not be considered to truly reflect the ability of the soil to resist fracture failure.

As discussed in Sect. 3, the fracture toughness of soil sample is mainly determined by the bending beam test and the compact tension test. The fracture toughness obtained by the two methods for soil samples with different a/W values have been extensively investigated by researchers (Ayad et al. 1997; Konrad and Cummings 2001; Nishimura and Shimizu 2004; Lakshmikantha et al. 2008, 2012; Wang et al. 2016, 2020). The results show that the fracture toughness of soil roughly decreases with increase of a/W, but there is a stable stage on that trend when bending beam test is used (Fig. 15). As mentioned above, fracture toughness should be a fixed value for a given state of a particular soil. Therefore, a/W of the test sample should be limited in order to obtain the real value of fracture toughness (Nishimura and Shimizu 2004; Wang et al. 2016, 2020).

4.2.2 Temperature

As for the influence of temperature on the fracture strength of soil, there are mainly researches on frozen soil. Frozen soil is composed of soil particles, ice inclusions, water (unfrozen water and tightly bound water) and gaseous inclusions (water vapor and air) (Lai et al. 2009, 2010). The difference between frozen soil and unfrozen soil is the existence of ice in the former (Chang and Liu 2013). The fracture parameters of frozen soil are strongly sensitive to ambient temperature. Many investigations have been performed on the fracture of frozen soils. (Li et al. 2000; Li and Yang 2000; Konrad and Cummings 2001; Liu and Liu, 2011). Generally, frozen soils are brittle at lower temperatures, and elastic–plastic at higher temperatures. As presented in Fig. 16, the values of K_{IC} and K_{IIC} increase as temperatures drop. This means that the strength of frozen soils increases as temperature decreases. Lowering of ambient temperature increases the strength and fracture toughness of a frozen soil. The reason is that the existence of ice will greatly increase the cohesion among particles.

4.2.3 Loading rate

In geotechnical engineering practice, rarely are external loads applied instantaneously but tend to increase. For this reason, some researchers have studied the influence of loading rate on the soil fracture patterns (Li et al. 2000; Li and Yang, 2000; Liu and Liu, 2011). As shown in Fig. 17a–b, the values of both K_{IC} and K_{IIC} grow as the loading rate increases in the early stage. With increase loading time, fracture toughness becomes less sensitive to increase loading rate.

Apart from the test-related factors discussed above, some researchers have also conducted a series of investigations on other significant factors, including soil sample thickness and notch crack angle (Liu and Liu 2011; Wang et al. 2020). Wang et al. (2020) used semi-circular samples with different thicknesses to perform three-point bending tests and found that the value of fracture toughness slightly decreases with increase in thickness and stabilizes after the thickness is greater than 50 mm. The small differences observed justify the consideration of fracture toughness as being a material characteristic. Thus, the method proposed by Wang et al. (2007a) to remove the influence of specimen self-weight on the experimental results is practicable.

During compression process, the soil undergoes bending failure and compression failure. Under certain conditions, the influence of compressive fracture on the soil is dominant. In order to study the mechanical characteristics of the compressive fracture of the soil, Liu and Liu (2011) used compact compression samples with different tilted wing crack angles to perform uniaxial unconfined compression fracture tests (shown in Fig. 12b). As the tilted wing crack angle increases, the value of K_{IC} and K_{IIC} show two different growth trends. The values of K_{IC} and K_{IIC} increase linearly and logarithmically with the increase in crack angle, respectively.

5 Soil cracking model based on fracture mechanics

The existence of microcracks and grains within a soil leads to stress concentrations, which can result in the failure of the soil. In a soil sample, once the surface energy of the expanding crack is balanced with the elastic potential energy released around the crack, the initiation and propagation of the crack will occur (Griffith et al. 1924). Fracture mechanics was originally applied to study the problem of tensile cracking of soils. Defects in the interior of heterogeneous soils lead to decreased strength, and the stress concentrations generated at tips of microcracks cause them to develop into visible macrocracks (Hallett et al. 1995; Lima and Grismer 1994; Hallett and Newson, 2001; Prat et al. 2008).

5.1 Linear elastic fracture mechanics LEFM

LEFM is often used to construct the soil desiccation cracking prediction model. During the soil cracking process, decrease in potential energy due to the release of tensile stress is equal to the increase in surface energy because of increase in crack surface area:

Table 3 Influence of the test-related factors on soil fracture parameters

Test-related factors	Variation component and range	Fracture parameters	Research results	References
The ratio of initial crack length to specimen width	0.381, 0.476, 0.667 (initial crack length: 40 mm, 50 mm, 70 mm; specimen width: 105 mm)	K_{IC}, G_C	K_{IC} and G_C value decreases as the initial crack length increases	Ayad et al. (1997)
	0.381, 0.524, 0.667 (initial crack length: 40 mm, 55 mm, 70 mm; specimen width: 105 mm)	K_{IC}	K_{IC} value decreases as the initial crack length increases	Konrad and Cummings (2001)
	1. 0.143, 0.179, 0.214, 0.250, 0.286, 0.429, 0.571 (initial crack length: 10.0, 12.5, 15.0, 17.5, 20.0, 30.0, 40.0 mm; specimen diameter 70.0 mm) 2. 0.143, 0.125, 0.111 (initial crack length: 10 mm; specimen diameter: 70.0, 80.0, and 90.0 mm)	K_{IC}	K_{IC} value increased until the ratio of initial crack length and diameter become 0.143, but it maintained a constant value when the ratio of initial crack length and diameter less than 0.143	Nishimura and Shimizu (2004)
	1. Medium specimen: 0.4, 0.6, 0.8 (initial crack length: 10, 15, 20 mm; specimen width: 25 mm) 2. Big specimen:0.4, 0.6, 0.8 (initial crack length: 20, 30, 40 mm; specimen width: 50 mm)	K_{IC}, G_C	K_{IC} value increases with decrease in initial crack length, G_C is a material constant for a given moisture content	Lakshmikantha et al. (2008, 2012)
	1. Small specimen: 0.2, 0.3, 0.4, 0.5, 0.6, 0.7, 0.8 (initial crack length: 10, 15, 20, 25, 30, 35, 40 mm; specimen width: 50 mm) 2. Big specimen: 0.125, 0.250, 0.375, 0.500, 0.625, 0.750, 0.875 (initial crack length: 10, 20, 30, 40, 50, 60, 70 mm; specimen width: 80 mm)	K_{IC}	For the small size specimen, the limit of crack depth is about the ratio of initial notch length to specimen width is 0.3 ~ 0.6, but for the small size specimen, the limit is about the ratio of initial notch length to specimen width is 0.25 ~ 0.625	Wang et al. (2016, 2020)
Temperature	-18, -16, -5, -2℃	K_{IIC}	K_{IIC} value increases linearly as temperature drops	Li et al. (2000)
	-15, -10, -7, -5, -2℃	K_{IC}	K_{IC} value increases linearly as temperature drops	Li and Yang (2000)
	-5, -2℃	K_{IC}	K_{IC} value increases as temperature drops	Konrad and Cummings (2001)
	-15, -10, -5℃	K_{IC}, K_{IIC}	K_{IC} and K_{IIC} increase exponentially as the temperature drops	Liu and Liu (2011)
Loading rate	5, 40, 120, 200 N/s	K_{IIC}	K_{IIC} is less sensitive to loading rate within the range of loading rate = 5 ~ 200 N/s	Li et al. (2000)
	1, 5, 40, 200, 500, 2000 N/s	K_{IC}	K_{IC} value increases as loading rate increases	Li and Yang (2000)
	1, 5, 10, 50, 100 mm/min	K_{IC}, K_{IIC}	Both K_{IC} and K_{IIC} exhibit logarithmic growth as the loading rate increases	Liu and Liu (2011)
Specimen thickness	20 mm, 35 mm, 50 mm, 65 mm	K_{IC}	K_{IC} value decreases as specimen thickness increases and tends to be stable when specimen thickness ≥ 50 mm. K_{IC} values can be regarded as a constant due to the small difference	Wang et al. (2020)
Tilted wing crack angle	15°, 25°, 35°, 45°	K_{IC}, K_{IIC}	As the tilted angle of the crack increases, the value of K_{IC} exhibits a linear growth pattern, and the value of K_{IIC} grows logarithmically	Liu and Liu (2011)

K_{IC} Mode-I fracture toughness, K_{IIC} Mode-II fracture toughness, G_C Critical energy release rate

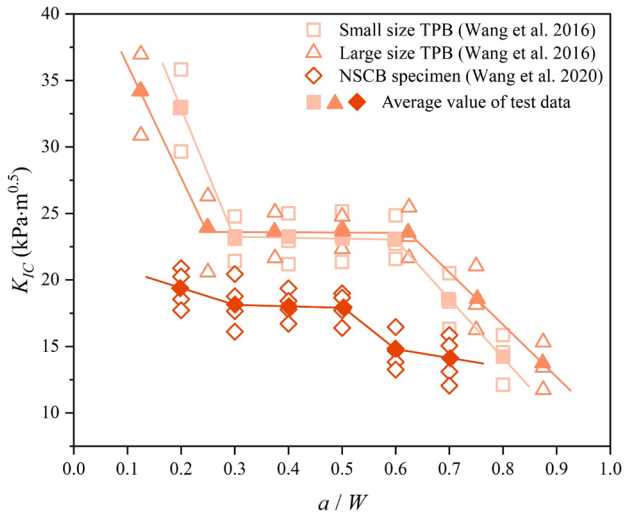

Fig. 15 The dependence of fracture toughness on the ratio of initial crack length to specimen width

$$\delta U \geq \delta U_{SE} \tag{44}$$

where δU is the reduced potential energy and δU_{SE} is the increased surface energy. The expression of critical stress based on Griffith energy criterion is:

$$\sigma_0 = \sigma_c \tag{45}$$

where σ_0 is the fracture driving force; σ_c is the fracture resistance, $\sigma_c = \sqrt{4\eta Y/\pi a}$, η is the surface energy per unit area, Y is the Young's modulus.

Soil desiccation cracking is more in accordance with the crack mode I Morris et al. (1992) proposed a model that combines crack depth, the soil mechanical properties and matric suction profile to predict the depth of the cracks and onset of soil secondary cracking:

$$\begin{cases} cK_I^1 = -0.4385\left(\frac{v}{1-v}\gamma_d + \frac{1-2v}{1-v}\frac{S_0}{h}\right)A^{1.5} \\ K_I^2 = 1.1215\left(\frac{v}{1-v}\gamma_d A - \frac{1-2v}{1-v}S_0\left(1-\frac{A}{h}\right)\right)A^{0.5} \\ K_I^3 = \left(\frac{1-2v}{1-v}\left(S_0\left(1-\frac{A}{h}\right)+\gamma_w(A-h)\right)+\frac{v}{1-v}(\gamma_s-\gamma_d)(A-h)\right)g\left(\frac{Z}{A}\right) \end{cases} \tag{46}$$

where S_0 is the surface suction; h is the depth to water table; A is the half length of internal crack; Z is the depth variable; γ_d is the unit weight of pore water, γ_s is the unit weight of saturated soil, γ_d is the unit weight of dry soil. In order to get the crack depth under critical conditions, fracture toughness K_{IC} should be determined when the crack initiated and developed in the soil:

$$K_{IC} = \frac{-2\xi E_c}{1-\nu^2} \tag{47}$$

where ξ is the specific surface energy, E_c is the compression modulus.

Konrad and Ayad (1997b) pointed out that the ultimate crack depth depends on the tensile stress distribution on both crack sides and the value of the stress intensity factor, which varies with the length of the crack. In order to use LEFM to predict the depth of soil cracks, two assumptions were made: the actual tensile stress distribution is linearly applied on both sides of the crack; and the stress intensity factor corresponds to the trapezoidal tensile stress distribution:

$$K_{I.trap} = K_{I.rect} - K_{I.tria} \tag{48}$$

where $K_{=1*\mathrm{ROMAN}.\mathrm{trap}}$ is stress intensity factors that corresponds to a trapezoidal tensile stress distribution, $K_{=1*\mathrm{ROMAN}.\mathrm{rect}}$ is the stress intensity factors that corresponds to a uniform tensile stress distribution, $K_{=1*\mathrm{ROMAN}.\mathrm{tria}}$ stress intensity factors corresponding to a triangular tensile stress distribution. In the case of initial soil cracks under the premise of ignoring gravitational stresses, the ultimate crack depth can be expressed as (Lachenbruch 1961):

$$\alpha_1\left(\frac{b}{a}\right)\sigma_t\sqrt{a} - \alpha_2\left(\frac{b}{a}\right)\left(\sigma_t - \sigma_3(b)\right)\sqrt{a} = K_{IC} \tag{49}$$

where σ_t is tensile strength, σ_3 is lateral total stress, b is the depth over which the tensile stress is applied to the crack walls, α_1 and α_2 are coefficients depending on the given values of a and b, as shown in Fig. 18.

Lakshmikantha et al. (2012) performed laboratory experiments on samples of different thicknesses and sizes, and the results indicated that soil cracking has obvious sample size effects. Although the initiation of soil cracks

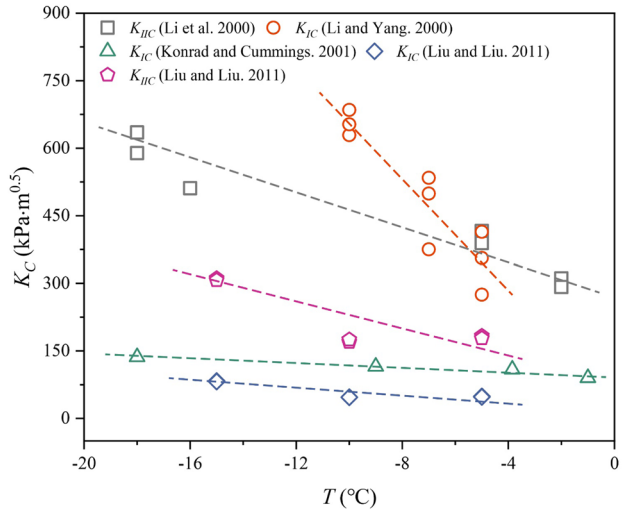

Fig. 16 The dependence of fracture toughness on temperature

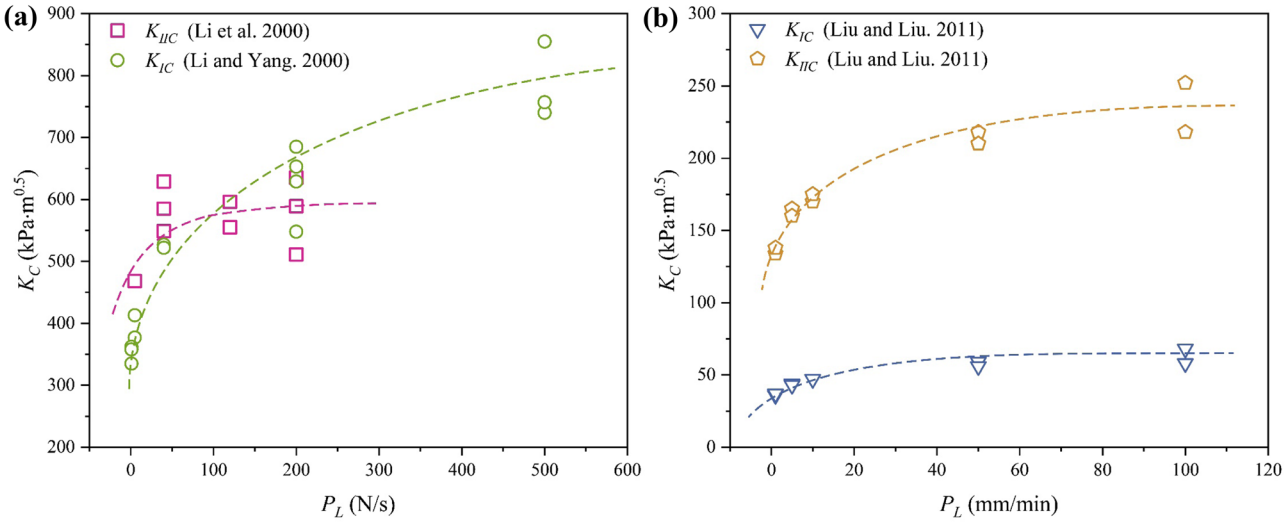

Fig. 17 The dependence of fracture toughness on loading rate. (**a**) stress controlled tests; (**b**) strain controlled tests

can be explained by the effective stress theory of classical soil mechanics, the development and propagation of soil cracks appears to be driven by energy. An indirect method of measuring the total length of a crack on the basis of LEFM was adopted to estimate the average cracking stress σ_a

$$\sigma_a = \sqrt{\frac{G_{IC}E}{\pi a}} \tag{50}$$

The size-effect law proposed by Bazant (1984) can be expressed as:

$$\sigma_a = \psi\sigma_t\left(1+\frac{d}{\lambda_0 d_0}\right)^{-0.5} \tag{51}$$

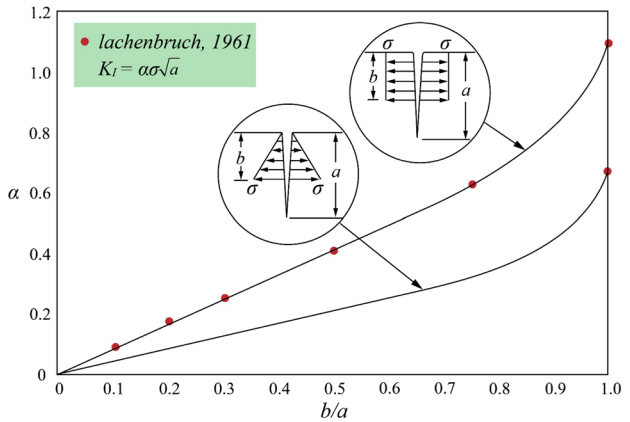

Fig. 18 Stress intensity functions for uniform and linear stress distributions (Konrad and Ayad 1997b)

where d is the characteristic dimension of specimen, d_0 is a reference dimension, ψ and γ_0 are parameters that can be determined from a linear regression analysis. The experiments performed by Lakshmikantha et al. (2012) could validated Eq. (51), thus proving that LEFM can be adequately accurate in explaining the process of development and propagation of soil desiccation cracks. After measuring the tensile strength and fracture toughness of the samples in previous published work, the following empirical relationship was proposed (Lakshmikantha et al. 2008, 2012; Prat et al. 2008):

$$K_{IC} = \alpha_t\sigma_t^n \tag{52}$$

where α_1 and n are the fitting proportionality coefficient. However, many researchers have performed a series of experiments to study the relationship between tensile strength and fracture toughness and pointed out that the two parameters have a good linear fit as expressed in Eq. (53) (Bhagat 1985; Harison et al. 1994; Wang et al. 2007b, 2020; Cao 2018).

$$K_{IC} = \alpha_t\sigma_t \tag{53}$$

These experimental results and curve fitting results are shown in Fig. 19. These results indicate that although fracture toughness and tensile strength of different soils have high linear correlation, there are also large differences in the values of proportionality coefficient and the determination coefficient. These observations may be due to differences in soil type and testing method, which is same as the measurement of tensile strength (Trabelsi et al. 2018). More experiments should be performed to unravel the reason for observed difference.

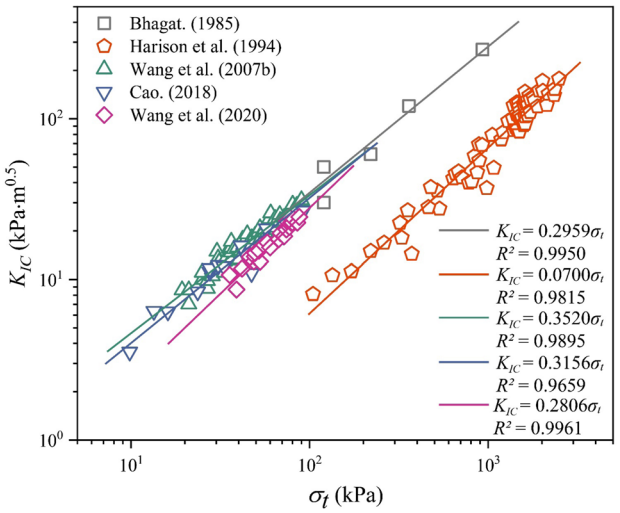

Fig. 19 Relationships between fracture toughness and tensile strength

5.2 Elastic plastic fracture mechanics EPFM

As discussed in Subsection 5.1, LEFM-based research assumes that the process of soil failure is a thermodynamic equilibrium process. This implies that the mechanical energy applied to the fracturing soil is equivalent to the energy required for soil cracking. For the linear elastic model of the soil cracking, the increase in mechanical energy dU will be converted into the increase in internal energy of the soil dw and the w is elastic and fully recoverable, which can be defined as $dU = dw_{el}$ (elastic energy w_{el}). When the external stress is removed, the soil can return to its original state. However, the assumption of this model fails to take into account the fact that a large amount of unrecoverable energy (plastic energyw_{pl}) in the soil cracking process is dissipated. The w_{pl} is mainly used for plastic processes including the soil particles rearrangement, the soil inter-particle friction and the debonding of inter-particle bonds (Abu-Hejleh and Znidarčić 1995).

In the EPFM model developed by Hallett and Newson (2005), the external energy is mainly decomposed into two parts, recoverable elastic energy w_{el} and irrecoverable plastic energy w_{pl}. When the crack propagates, sufficient energy is needed to break the soil inter-particle bonds at the crack tip:

$$dU = dw_{el} + dw_{pl} + d\Phi \tag{54}$$

Where $d\Phi$ is the energy required for the destruction of the soil structure $d\Phi = 2B\gamma_0 da$, which depends on the specific surface energy γ_0 and the increased surface area $2Bda$ (the amount of crack growth da and the crack thickness B) because of soil cracking. Therefore, Eq. (54) can be transformed into:

$$\frac{d\left(U - w_{el}\right)}{Bda} = \frac{d\left(w_{pl} + \Phi\right)}{Bda} \tag{55}$$

The energy source of soil crack propagation is the driving force of crack D, expressed as:

$$C \equiv \frac{d\left(U - w_{el}\right)}{Bda} \tag{56}$$

The energy sink of soil crack propagation is the energy dissipation rate C, expressed as:

$$D \equiv \frac{d\left(w_{pl} + \Phi\right)}{Bda} \tag{57}$$

Once the soil cracks begin to develop, the energy source and sink must be equal, $C = D$.

In the EPFM model, the J integral is an important parameter. First introduced by Rice (1968), it can be conveniently used to express the potential energy change rate during soil crack propagation at different water contents. Being that the J integral can be applied to evaluate the change of elastic potential energy and plastic potential energy, it is reasonable to use this parameter to analyze the elastic–plastic transition during crack development. Costa et al. (2012, 2013b, 2016) proposed a new ring test method to determine the elasto-plastic fracture behavior of soil from the form of J integral. Different from the fracture parameters measured by the load control test, the J integral value measured from the natural drying ring test, is more suitable for use in the analysis of soil desiccation cracking.

The LEFM model is applicable to the problem of soil tension crack under stress. Although there is a certain gap between some assumptions in the theoretical model and the actual situation, the predicted soil crack depth has a certain reference in theory (Miller et al. 2016). A major disadvantage of the LEFM model is that the soil is not a brittle and linear elastic material, and energy dissipation from other processes (such as elastic mismatch, inter-particle friction, and micro-cracks) may be substantial (Hallett et al. 1995). Another limitation is that the LEFM model only considers the propagation of an individual crack and ignores the interactions among multiple cracks (Konrad and Ayad 1997b). These limitations lead to discrepancies between the theoretical predictions and the observed cracks in the actual situation. The EPFM model is an improvement on the LEFM model through consideration of the plastic deformation processes and irreversible plastic energy dissipation during soil cracking, which are more in accordance with the actual situation. Researchers have not only put forward that the soil cracking should be a non-linear fracture behavior (Vo et al. 2017) and created a process zone for plastic energy dissipation (Kendall and Weihs 1992), but have also proposed a new ring for testing the J integral parameter that

is used to evaluate the elastoplastic fracture characteristics of natural soil during desiccation cracking (Costa et al. 2012, 2013b, 2016). However, there is still the challenge of accurately quantifying the parameters needed for use of the EPFM model and differentiating the elastic processes form the plastic processes during soil cracking. At present, the development of most LEFM and EPFM models is limited to numerical simulations due to lack of relevant laboratory and field confirmatory experiments. So, there is not enough experimental data to verify the rationality of the models. However, the application of LEFM and EPFM theory to soil cracking research has a great significance in existing soil cracking theory and provides a theoretical basis for the development of related cracking models in the future.

6 Numerical simulations of soil cracking based on fracture mechanics

To avoid the shortcomings of experiments, numerical simulation methods have been one of the important ways of studying cracking of soils (Sanchez et al. 2014). Due to the complexity of cracking initiation and propagation processes in soils, the fundamental mechanisms of soil cracking are still under investigation. The accuracy and reliability of most numerical models are under question. Current numerical simulation methods of soil cracking that are based on fracture mechanics can be categorized into two major groups: LEFM and cohesive crack method.

Lee et al. (1988) proposed a finite element model based on LEFM to predict crack propagation in brittle soil. The model splits a single node into two different nodes to represent the separation of material on both sides of the soil crack. The critical energy release rate is used as the material constant for soil tension cracks (Fig. 20). It is worth pointing out that the model has been verified with two field cases, including a soft soil embankment and an excavated slope.

Konrad et al. (1997b) proposed a highly idealized analytical model based on LEFM for predicting the spacings among the soil desiccation cracks and describing the phenomenon of crack propagation. This model can be applied to the dry shrinkage cracking characteristics of simulated mud, natural consolidated soil and compacted clay. Its predictions are in agreement with soil cracking experiments performed in an Australian coal mine tailings deposit.

Juárez-Luna et al. (2014) used a two-dimensional fracture mechanics finite element program based on the LEFM theory, to simulate soil crack initiation and propagation, and verified the control effect of critical stress intensity factor on soil crack development. The crack depths obtained with the numerical model had good agreement with field geotechnical data from the Valley of Mexico.

However, some researchers have indicated that LEFM may be more suitable for brittle soils. LEFM assumes infinite tensile stress at the crack tip, which is not valid when the material has limited tensile strength and displays significant plastic behavior around the crack process zone (Amarasiri and Kodikara 2011). The cohesive crack model is an attractive model for plastic soils that incorporate the main physical features of soil, particularly, fracture energy requirements and nonlinearity. Therefore, the cohesive crack method is more appropriate than LEFM for analyses of cracking of high moisture content soils due to the likely occurrence of the plasticity cracking zone (Amarisiri et al. 2014). The basic principle of the cohesive crack model is that the bridging stress σ during the opening the two crack faces, is a function of the crack opening near the crack tip (called the fracture process zone (FPZ) (Carpinteri and Colombo 1989)). The bridging stresses of a cohesive crack is shown in Fig. 21. This relationship between the bridging stress σ and the cohesive crack opening displacement w can be expressed as shown in Eq. (58).

$$\sigma = \mathrm{f}(w) \tag{58}$$

As the relative displacement between the two soil crack faces increases from zero to w, the crack bridging tensile stress gradually decreases from the tensile strength σ_t to zero at the same time.

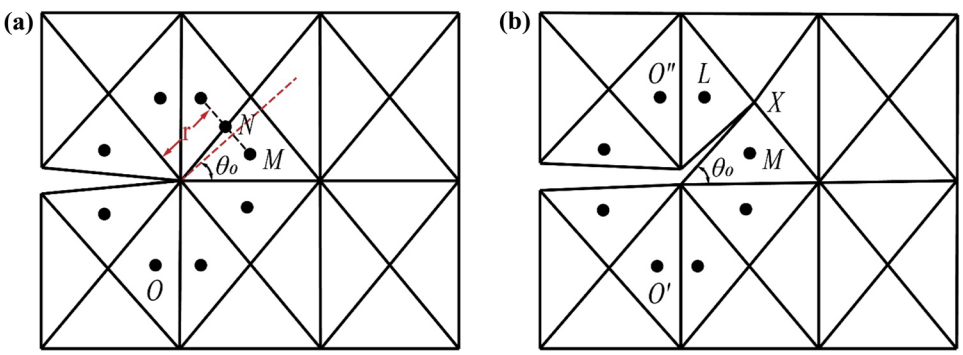

Fig. 20 Proposed crack propagation mechanism: (**a**) before crack increment; (**b**) after crack increment (Lee et al. 1988)

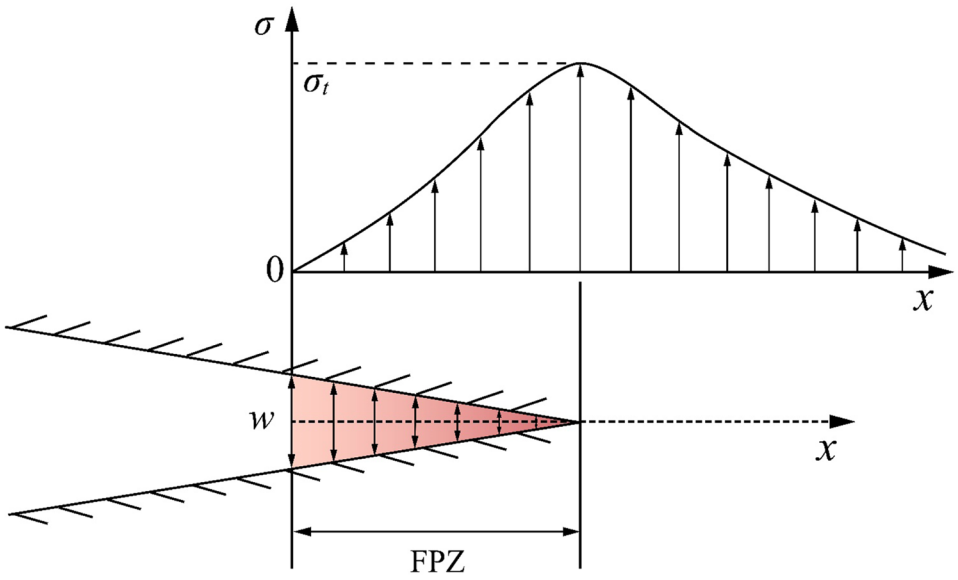

Fig. 21 Bridging stresses of cohesive crack (Amarasiri and Kodikara 2011)

Amarasiri and Kodikara (2011, 2013a, b) proposed a methodology that is based on cohesive crack method for numerical simulation of soil cracking. This mode does not have the requirement that an initial notch must be present and the bulk material must behave in a linear elastic manner. This method has been validated in some experiments, including a tension test with a rectangular cross section, a laboratory linearly constrained desiccation test, a notched three-point bend beam, a restrained ring, test a compact tension test and a field desiccation test performed in Saint Alban, Canada (Amarasiri and Kodikara, 2011, 2013a, b; Amarisiri et al. 2014).

Gui et al. (2016) developed a mix-mode cohesive fracture model for simulating soil desiccation cracking by employing a hybrid continuum-discrete method, implemented using Universal Distinct Element Code (UDEC). The cohesive fracture model considers tension, compression and shearing behavior of bonds among soil grains. The model produces results that are consistent with laboratory test results and deal with multiple fracture and deformation problems. The simulation results of three final crack patterns with different soil thickness (4 mm, 8 mm, and 16 mm) are shown in Fig. 22.

Vo et al. (2017) built a cohesive damage-plasticity model to simulate the desiccation cracking of a clayey soil with consideration of soil hydraulic and mechanical behavior. This model can capture the initiation and propagation of soil cracks. Their results indicate that the model can reproduce trends observed in experiments (soil sample shrinkage, crack initiation and propagation, as shown in Fig. 23), and also enable investigation of the evolution of cracking soil mechanical parameters (stress, strain) and hydric state (suction, degree of saturation) at different soil specimen locations. In order to predict soil crack spacing and depth, a finite element code that enables incorporation of cohesive joint elements was used by Vo et al. (2019). From the results of numerical simulations, empirical correlations were developed to predict soil crack spacings and depths as functions of the surface suction on top of the soil, soil physical parameters and moisture evaporation rate. These results prove the validity of models with in situ experimental observations.

The cohesive zone model (CZM) was initially built to describe the plastic-zone beyond the crack tip (Barenblatt 1959). Pouya et al. (2019) developed the CZM by using finite element code to correctly predict the crack initiation and the ultimate

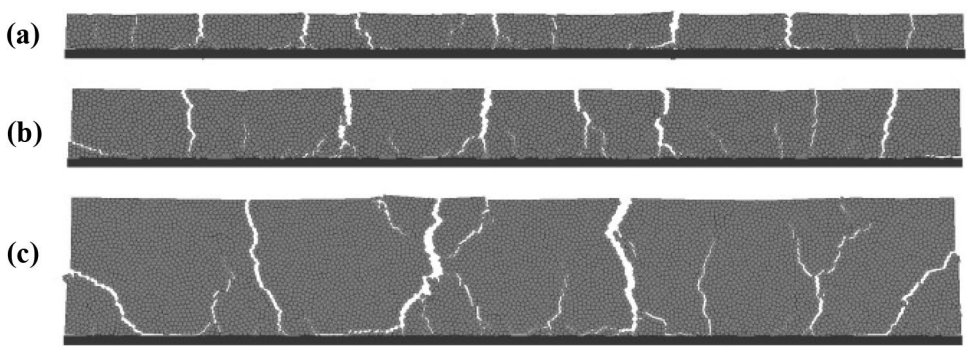

Fig. 22 The simulation results with different soil thickness. (**a**) 4 mm, (**b**) 8 mm, (**c**) 16 mm. All the three simulations with same soil-base strength, i.e., cohesion = 1.4 kPa, tensile strength = 0.7 kPa and friction angle = 5° (Gui et al. 2016)

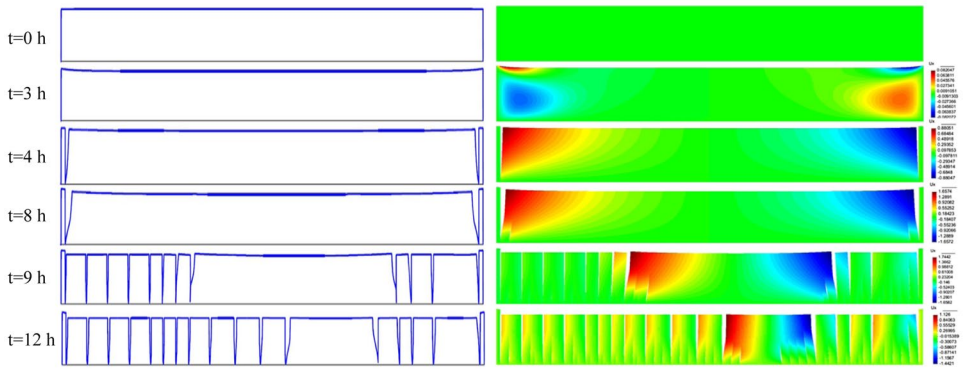

Fig. 23 (**a**) Description of the cracks observed at various moments and (**b**) distribution of horizontal displacement (Vo et al. 2017)

crack depth. The numerical analysis shows that the maximum dissipated energy per unit crack depth can predict the soil desiccation crack depth and its related spacing. The CZM were successfully used to reproduce soil crack evolution and strain localization changes in the different fracture ductility clay beams flexural test (Hu et al. 2020).

Therefore, numerical models that are based on cohesive crack method can been valuable tools in soil cracking modeling with laboratory and field desiccation tests. The LEFM have been developed to study the propagation of a single crack. It can successfully predict crack depth from the soil suction and other mechanical parameters. However, the LEFM may be more suitable for brittle soils, rather plastic soils (Hallett and Newson 2005). On the other hand, the cohesive crack model is an attractive model for plastic soils because it incorporates the main physical features of a soil, including fracture energy and material nonlinearity. It is noted that the cohesive crack method is a calculation method based on EPFM that is widely used in the study of crack propagation (Ozenc et al. 2014). Meanwhile, the cohesive crack method has strong adaptability and can solve many nonlinear and large deformation problems. Compared with the stress intensity factor, the existence of cohesion keeps the crack tip to maintain a closing tendency, which can reduce or eliminate the stress singularity to a certain extent (van der Meer et al. 2012). Although the numerical simulation of soil cracking based on fracture mechanics can effectively predict the depth and spacing of soil desiccation cracks, the limited validation and verifications with field data as well as soil inhomogeneity make it necessary to test them more before wide application in geotechnical practice.

7 Conclusions and future works

This review synthesizes the past research efforts devoted to the experimental investigations and applications of fracture mechanics in soil cracking. This section presents concluding remarks and some outlooks requiring further investigations.

Five main test methods have been used to analyze soil fracture processes and parameters. It is obvious that each method has its advantages and limitations. Although the three-point bending test and the four-point bending test are very convenient methods of measuring soil fracture parameters, the self-weight of soil samples will affect the accuracy of the fracture parameters. While the compact tension test can overcome the influence of sample self-weight on the test results, failure of the soil loading point tends to precede the soil sample fracture because of the low tensile strength of most soils. The ring test is mainly used to obtain the value of J integral on the basis of EPFM, which has been widely applied in stress analyses. However, the ring test is a complicated measurement method when applied to soil cracking, and the test conditions are relatively strict, thereby rendering it unamenable to frequent use. The compression test is mainly applicable to frozen soils that exhibit higher strength. Pre-existing cracks and external loading of the compression samples influence the accuracy of fracture parameters of soil specimens with lower strength. Adjustment and standardization of test procedures, and development of easy-to-operate test devices are urgently needed for measurements of soil fracture parameters. This would enhance the convenience of replication of experiment for comparison, validation and verification of results of modeling.

The LEFM model is applicable to the problem of soil tension cracking under stress. Although there is a certain gap between some assumptions in the theoretical model and the actual situation, the predicted soil crack depth has reasonable rationale in theory. A major disadvantage of the LEFM model is that the soil is not a brittle and linear-elastic material, and energy dissipation from other processes lead to discrepancies between the theoretical predictions and experimental observations. The EPFM model is an improvement on the LEFM model through considerations of soil plasticity and irreversible plastic energy dissipation during soil cracking. These considerations are more reflective of the actual situation of soil cracking. However, it is still a challenge to accurately quantify the parameters that are incorporated

into the EPFM model and distinguish between the elastic and plastic deformation processes during soil cracking. At present, the validation and verifications of most LEFM and EPFM models is limited to numerical simulations. Lack of relevant laboratory and field confirmatory experiments is a problem. However, the application of LEFM and EPFM theory in soil cracking research has high utility as regards the provision of the theoretical basis for the development of related cracking models in the future for field application.

Classical fracture mechanics is mainly applicable to brittle materials, while soil will show two states of brittleness and plasticity with the change of water content. Therefore, EPFM will be a key factor in using fracture mechanics to propose soil cracking models. Although fracture mechanics has made some progress in explaining soil crack propagation, there are still shortcomings in accurately judging the initiation time and position of soil crack. Hence, it is necessary to combine soil mechanics and fracture mechanics to complete a theoretical model to explain soil crack initiation and propagation. It is significant to fully understand the connections between soil microstructure, plasticity and cracking. The current research on fracture mechanics in soil cracking is mainly limited to laboratory tests, while the research results of field tests and numerical simulations are obviously insufficient. Although in-situ tests have problems such as time-consuming, laborious and high cost, such tests have an irreplaceable effect on the study of the essential laws of soil cracking. In addition, so far, the soil microstructure is rarely used in the research of soil fracturing. How to establish a connection between the quantitative parameters of the microstructure and the soil fracture parameters will be a challenging topic in the future.

Acknowledgements This work was supported by the National Key Research and Development Program of China (Grant No. 2019YFC1509902, 2020YFC1808101), National Natural Science Foundation of China (Grant No. 41925012, 41902271, 41772280), and the Fundamental Research Funds for the Central Universities.

References

Abd El-Halim AA (2017) Image processing technique to assess the use of sugarcane pith to mitigate clayey soil cracks: Laboratory experiment. Soil till Res 169:138–145

Abou Najm MR, Jabro JD, Iversen WM, Mohtar RH, Evans RG (2010) New method for the characterization of three-dimensional preferential flow paths in the field. Water Resour Res 46:W02503

Abuhejleh AN, Znidarcic D (1995) Desiccation theory for soft cohesive soils. J Geotech Eng-Asce 121(6):493–502

Albrecht BA, Benson CH (2001) Effect of desiccation on compacted natural clays. J Geotech Geoenviron 127(1):67–75

Al-Jeznawi D, Sanchez M, Al-Taie AJ (2021) Using image analysis technique to study the effect of boundary and environment conditions on soil cracking mechanism. Geotech Geol Eng 39:25–36

Alonso E, Gens A, Lloret A, Delahaye C (1995) Effect of rain infiltration on the stability of slopes. Proc. 1st Int. Conf. Unsaturated Soils, Paris 1:241–248

Aluko OB, Chandler HW (2006) A fracture strength parameter for brittle agricultural soils. Biosyst Eng 93:245–252

Amarasiri A, Kodikara J (2011) Use of material interfaces in DEM to simulate soil fracture propagation in mode I cracking. Int J Geomech 11:314–322

Amarasiri AL, Costa S, Kodikara JK (2011) Determination of cohesive properties for mode I fracture from compacted clay beams. Can Geotech J 48:1163–1173

Amarasiri AL, Kodikara JK (2013a) Numerical modeling of desiccation cracking using the cohesive crack method. Int J Geomech 13:213–221

Amarasiri AL, Kodikara JK (2013b) Numerical modelling of a field desiccation test. Geotechnique 63:983–986

Amarisiri A, Shannon B, Kodikara J (2014) Numerical modelling of desiccation cracking in a restrained ring test. Can Geotech J 51:67–76

ASTM E399–83 (1983) Standard test method for plane-strain fracture toughness of metallic materials American Society for Testing and Materials, Philadelphia Annual Book of ASTM Standards

ASTM E399–20 (2020) Standard test method for linear-elastic plane-strain fracture toughness KIC of metallic materials. Annual book of ASTM standards. West Conshohocken

Ayad R, Konrad JM, Soulié M (1997) Desiccation of a sensitive clay: application of the model CRACK. Can Geotech J 34:943–951

Baker R (1981) Tensile strength, tension cracks, and stability of slopes. Soils Found 21:1–17

Barenblatt GI (1959) The formation of equilibrium cracks during brittle fracture. General ideas and hypotheses. Axially-symmetric cracks. J Appl Math Mech. 23(3):622–636

Bazant ZP (1984) Size Effect in Blunt Fracture-Concrete. Rock, Metal J Eng Mech-Asce 110:518–535

Bhagat RB (1985) Mode-i fracture-toughness of coal. Int J Mining Eng 3(3):229–236

Bhurke AS, Shin EE, Drzal LT (1997) Fracture morphology and fracture toughness measurement of polymer-modified asphalt concrete. Transport Res Rec(1590):23–33

Bishop A (1971) The influence of progressive failure on the choice of the method of stability analysis. Geotechnique 21(2):168–172

Cai WM, Murti V, Valliappan S (1990) Slope stability analysis using fracture-mechanics approach. Theor Appl Fract Mec 12(3):261–281

Cao KD (2018) Determination of Mode I fracture toughness, tensile strength and adhesion of compacted clays. Master's thesis Alberta, Canada: University of Calgary

Carpinteri A, Colombo G (1989) Numerical-analysis of catastrophic softening behavior (snap-back instability). Comput Struct 31(4):607–636

Chandler HW (1984) The use of non-linear fracture-mechanics to study the fracture properties of soils. J Agr Eng Res 29(4):321–327

Chang D, Liu JK (2013) Review of the influence of freeze-thaw cycles on the physical and mechanical properties of soil. Sciences in Cold and Arid Regions 5(4):457–460

Chaves FJP, da Silva LFM, de Moura MFSF, Dillard DA, Esteves VHC (2014) Fracture mechanics tests in adhesively bonded joints: A literature review. J Adhesion 90(12):955–992

Cherepanov GP (1967) The propagation of cracks in a continuous medium. J Appl Math Mech 31(3):503–512

Colombi T, Kirchgessner N, Iseskog D, Alexandersson S, Larsbo M, Keller T (2021) A time-lapse imaging platform for quantification of soil crack development due to simulated root water uptake. Soil Till Res 205:104769

Cordero JA, Useche G, Prat PC, Ledesma A, Santamarina JC (2017) Soil desiccation cracks as a suction-contraction process. Geotechnique Letters 7(4):279–285

Corte A, Higashi A (1960) Experimental research on desiccation cracks in soil, Research Report 66. In: Tech. Rep. US Army Snow Ice and Permafrost Research Establishment, Wilmette, Illinois

Costa S, Htike WY, Kodikara J, Xue JF (2016) Determination of j-integral for clay during desiccation. Environ Geotech 3(6):372–378

Costa S, Kodikara J (2012) Evaluation of j integral for clay soils using a new ring test. Geotech Test J 35(6):981–989

Costa S, Kodikara J, Shannon B (2013a) Salient factors controlling desiccation cracking of clay in laboratory experiments. Geotechnique 63(1):18–29

Costa S, Kodikara J, Xue J (2013b) J-integral as a useful fracture parameter for analysis of desiccation cracking in clayey soils. Coupled Phenomena in Environmental Geotechnics: From Theoretical and Experimental Research to Practical Applications:377–381

DeCarlo KF, Shokri N (2014) Salinity effects on cracking morphology and dynamics in 3-d desiccating clays. Water Resour Res 50(4):3052–3072

Demagistri A, Ledesma Villalba A, Cordero Arias JA, Moreno R, Prat Catalán P, Jacinto AC (2018). Effects of compaction on desiccation cracking of clayey soils. Proceedings 7th International Conference on Unsaturated Soils, pp 1273–1278

Di Carlo E, Chen CR, Haynes RJ, Phillips IR, Courtney R (2019) Soil quality and vegetation performance indicators for sustainable rehabilitation of bauxite residue disposal areas: A review. Soil Res 57(5):419–446

Dugdale DS (1960) Yielding of steel sheets containing slits. J Mech Phys Solids 8(2):100–104

Erdogan F, Sih GC (1963) On the crack extension in plates under plane loading and transverse shear. J Basic Eng 85:519–525

Fredlund DG (1987) Slope stability analysis incorporating the effect of soil suction. Slope Stability. Wiley Press, New Yok, pp 113–144

Goehring L, Nakahara A, Dutta T, Kitsunezaki S, Tarafdar S (2015) Desiccation cracks and their patterns: formation and modelling in science and nature. Wiley- VCH, Singapore, pp 349p

Griffith A (1924) The theory of rupture. In: First Int Cong Appl Mech:55–63

Guan JF, Li CM, Wang J, Qing LB, Song ZK, Liu ZP (2019) Determination of fracture parameter and prediction of structural fracture using various concrete specimen types. Theor Appl Fract Mec 100:114–127

Gui YL, Zhao ZY, Kodikara J, Bui HH, Yang SQ (2016) Numerical modelling of laboratory soil desiccation cracking using udec with a mix-mode cohesive fracture model. Eng Geol 202:14–23

Hallett PD, Dexter AR, Seville JPK (1995) The application of fracture mechanics to crack propagation in dry soil. Eur J Soil Sci 46(4):591–599

Hallett PD, Newson TA (2001) A simple fracture mechanics approach for assessing ductile crack growth in soil. Soil Sci Soc Am J 65(4):1083–1088

Hallett PD, Newson TA (2005) Describing soil crack formation using elastic-plastic fracture mechanics. Eur J Soil Sci 56(1):31–38

Han ZY, Weatherley D, Puscasu R (2018) Projected area-based strength estimation for jointed rock masses in triaxial compression. Comput Geotech 104:216–225

Harison JA, Hardin BO, Mahboub K (1994) Fracture-toughness of compacted cohesive soils using ring test. J Geotech Eng-Asce 120(5):872–891

Haynes RJ, Swift RS (1990) Stability of soil aggregates in relation to organic-constituents and soil-water content. J Soil Sci 41(1):73–83

Hewitt PJ, Philip LK (1999) Problems of clay desiccation in composite lining systems. Eng Geol 53(2):107–113

Hirobe S, Oguni K (2017) Modeling and numerical investigations for hierarchical pattern formation in desiccation cracking. Physica D 359:29–38

Hu CB, Wang L, Ling DS, Cai WJ, Huang ZJ, Gong SL (2020) Experimental and numerical investigation on the tensile fracture of compacted clay. Cmes-Comp Model Eng 123(1):283–307

Irwin GR (1957) Analysis of stresses and strains near the end of a crack traversing a plate. J Appl Mech 24:361–364

Janssen M, Zuidema J, Wanhill R (2004) Fracture mechanics, Spon Press, Taylor & Francis Group, Second Edition

Juárez-Luna G, Ayala G (2014) Application of fracture mechanics to cracking problems in soils. Open Constr Build Technol J 8(1):1–8

Julina M, Thyagaraj T (2020) Combined effects of wet-dry cycles and interacting fluid on desiccation cracks and hydraulic conductivity of compacted clay. Eng Geol 267

Kendall K, Weihs TP (1992) Adhesion of nanoparticles within spray-dried agglomerates. J Phys D Appl Phys 25(1a):A3–A8

Khalilpour S, BaniAsad E, Dehestani M (2019) A review on concrete fracture energy and effective parameters. Cement Concrete Res 120:294–321

Konrad JM, Ayad R (1997a) Desiccation of a sensitive clay: Field experimental observations. Can Geotech J 34(6):929–942

Konrad JM, Ayad R (1997b) An idealized framework for the analysis of cohesive soils undergoing desiccation. Can Geotech J 34(4):477–488

Konrad JM, Cummings J (2001) Fracture toughness of frozen base and subbase soils in pavement. Can Geotech J 38(5):967–981

Krisnanto S, Rahardjo H, Fredlund DG, Leong EC (2014) Mapping of cracked soils and lateral water flow characteristics through a network of cracks. Eng Geol 172:12–25

Kuai H, Lee HJ, Zi G, Mun S (2009) Application of generalized j-integral to crack propagation modeling of asphalt concrete under repeated loading. Transp Res Rec(2127):72–81

Lachenbruch A (1961) Depth and spacing of tension cracks. J Geophys Res 66(12):4273–5000

Lai YM, Jin L, Chang XX (2009) Yield criterion and elasto-plastic damage constitutive model for frozen sandy soil. Int J Plasticity 25(6):1177–1205

Lai YM, Yang YG, Chang XX, Li SY (2010) Strength criterion and elastoplastic constitutive model of frozen silt in generalized plastic mechanics. Int J Plasticity 26(10):1461–1484

Lakshmikantha MR, Prat PC, Ledesma A (2012) Experimental evidence of size effect in soil cracking. Can Geotech J 49(3):264–284

Lakshmikantha MR, Prat PC, Ledesma A (2018) Boundary effects in the desiccation of soil layers with controlled environmental conditions. Geotech Test J 41(4):675–697

Lakshmikantha MR, Prat PC, Tapia J, Ledesma A (2008) Effect of Moisture Content on Tensile Strength and Fracture Toughness of a Silty Soil. First European Conference on Unsaturated Soils, E-UNSAT 2008. Taylor & Francis, Durham, UK: pp 405–409

Lau I, Li CQ, Fu GY (2019) Prediction of time to corrosion-induced concrete cracking based on fracture mechanics criteria. J Struct Eng 145(8):04019069

Lee FH, Lo KW, Lee SL (1988) Tension crack development in soils. J Geotech Eng-Asce 114(8):915–929

Lenci S, Clementi F, Sadowski T (2012) Experimental determination of the fracture properties of unfired dry earth. Eng Fract Mech 87:62–72

Li HS, Yang HT (2000) Experimental investigation of fracture toughness of frozen soils. J Cold Reg Eng 14(1):43–49

Li HS, Yang HT, Liu ZL (2000) Experimental investigation of fracture toughness k-iic of frozen soil. Can Geotech J 37(1):253–258

Li JH, Zhang LM (2010) Geometric parameters and rev of a crack network in soil. Comput Geotech 37(4):466–475

Li JH, Zhang LM (2011) Study of desiccation crack initiation and development at ground surface. Eng Geol 123(4):347–358
Li JH, Zhang LM, Li X (2011) Soil-water characteristic curve and permeability function for unsaturated cracked soil. Can Geotech J 48(7):1010–1031
Li JH, Lu Z, Guo LB, Zhang LM (2017) Experimental study on soil-water characteristic curve for silty clay with desiccation cracks. Eng Geol 218:70–76
Lima LA, Grismer ME (1994) Application of fracture-mechanics to cracking of saline soils. Soil Sci 158(2):86–96
Lin ZY, Tang CS, Zeng H, Wang YS (2020) Laboratory characterization and discrete element modeling of desiccation cracking behavior of soils under different boundary conditions (in Chinese). Chinese J Geotech Eng 42:372–380
Lin XB, Xue JL (1985) The determination of KI and KII for single edge crack beam subjected to combined loading using J-integral. Proceedings of the Fracture mechanism Program and Related Papers Present at the International Conference and Exposition on Fatigue, Corrosion Cracking, Fracture Mechanics and Failure Analysis, Salt Lake City, Utah, pp 157–163
Liu XZ, Liu P (2011) Experimental research on the compressive fracture toughness of wing fracture of frozen soil. Cold Reg Sci Technol 65(3):421–428
Luo PF, Chuang CK, Chao YJ (2003) Measurement of j integral by shadow spot generated from out-of-plane displacement. Opt Eng 42(12):3433–3442
Miller CJ, Mi H, Yesiller N (1998) Experimental analysis of desiccation crack propagation in clay liners. J Am Water Resour as 34(3):677–686
Miller GA, Hassanikhah A, Varsei M (2016) Desiccation crack depth and tensile strength in compacted soil. Unsaturated Soil Mechanics-from Theory To Practice:79–87
Mindess S, Lawrence FV, Kesler CE (1977) J-integral as a fracture criterion for fiber reinforced-concrete. Cement Concrete Res 7(6):731–742
Morris PH, Graham J, Williams DJ (1992) Cracking in drying soils. Can Geotech J 29(2):263–277
Murray I, Tarantino A (2019) Mechanisms of failure in saturated and unsaturated clayey geomaterials subjected to (total) tensile stress. Geotechnique 69(8):701–712
Narani SS, Abbaspour M, Hosseini SMMM, Aflaki E, Nejad FM (2020) Sustainable reuse of waste tire textile fibers (wttfs) as reinforcement materials for expansive soils: With a special focus on landfill liners/covers. J Clean Prod 247:119151
Newman JC, James MA, Zerbst U (2003) A review of the CTOA/CTOD fracture criterion. Eng Fract Mech 70(3–4):371–385
Nishimura S, Shimizu H (2004) A study of the measurement of fracture toughness in cohesive soil - relationship between the size of initial crack and diameter of specimen. Paddy Water Environ 2(1):27–32
Omidi GH, Thomas JC, Brown KW (1996) Effect of desiccation cracking on the hydraulic conductivity of a compacted clay liner. Water Air Soil Poll 89(1–2):91–103
Ozenc K, Kaliske M, Lin GY, Bhashyam G (2014) Evaluation of energy contributions in elasto-plastic fracture: A review of the configurational force approach. Eng Fract Mech 115:137–153
Peron H, Delenne JY, Laloui L, El Youssoufi MS (2009a) Discrete element modelling of drying shrinkage and cracking of soils. Comput Geotech 36(1–2):61–69
Peron H, Hueckel T, Laloui L, Hu LB (2009b) Fundamentals of desiccation cracking of fine-grained soils: Experimental characterisation and mechanisms identification. Can Geotech J 46(10):1177–1201
Poulsen TG, Cai WL, Garg A (2020) Water evaporation from cracked soil under moist conditions as related to crack properties and near-surface wind speed. Eur J Soil Sci 71(4):627–640
Pouya A, Vo TD, Hemmati S, Tang AM (2019) Modeling soil desiccation cracking by analytical and numerical approaches. Int J Numer Anal Met 43(3):738–763
Prat PC, Ledesma A, Lakshmikantha MR, Levatti H, Tapia J (2008) Fracture mechanics for crack propagation in drying soils. In: Proceedings of the 12th International Conference of the International Association for Computer Methods and Advances in Geomechanics, IACMAG. Vol. 12: pp 1060–1067
Qu J, Ma J, Yang B (2020) Influence of boundary conditions on cracking of sanxingdui moon bay city wall. Adv Civ Eng 2020:1531873
Rayhani MHT, Yanful EK, Fakher A (2007) Desiccation-induced cracking and its effect on the hydraulic conductivity of clayey soils from iran. Can Geotech J 44(3):276–283
Rice JR (1968) A path independent integral and the approximate analysis of strain cncentrations by notches and cracks. J Appl Mech-T ASME 35:379–386
Rice J, Paris P, Merkle J (1973) Some further results of J-integral analysis and estimates, Progress in flaw growth and fracture toughness testing. ASTM International, Philadelphia, Pa
Robinson JD, Vahedifard F (2016) Weakening mechanisms imposed on california's levees under multiyear extreme drought. Clim Change 137(1–2):1–14
Sanchez M, Atique A, Kim S, Romero E, Zielinski M (2013) Exploring desiccation cracks in soils using a 2d profile laser device. Acta Geotech 8(6):583–596
Sanchez M, Manzoli OL, Guimaraes LJN (2014) Modeling 3-d desiccation soil crack networks using a mesh fragmentation technique. Comput Geotech 62:27–39
Scavia C (1990) Fracture-mechanics approach to stability analysis of rock slopes. Eng Fract Mech 35(4–5):899–910
Shin H, Santamarina JC (2011) Desiccation cracks in saturated fine-grained soils: Particle-level phenomena and effective-stress analysis. Geotechnique 61(11):961–972
Shokri N, Zhou P, Keshmiri A (2015) Patterns of desiccation cracks in saline bentonite layers. Transport Porous Med 110(2):333–344
Sih GC (1974) Strain energy density factor applied to mixed mode crack problems. Int J Fracture 10(3):305–321
Sima J, Jiang MJ, Zhou CB (2014) Numerical simulation of desiccation cracking in a thin clay layer using 3d discrete element modeling. Comput Geotech 56:168–180
Skempton A, Schuster R, Petley D (1969) Joints and fissures in the london clay at wraysbury and edgware. Geotechnique 19(2):205–217
Song WK, Cui YJ (2020) Modelling of water evaporation from cracked clayey soil. Eng Geol 266:105465
Stirling RA, Toll DG, Glendinning S, Helm PR, Yildiz A, Hughes PN, Asquith JD (2020) Weather-driven deterioration processes affecting the performance of embankment slopes. Géotechnique:1–13
Sture S, Alqasabi A, Ayari M (1999) Fracture and size effect characters of cemented sand. Int J Fracture 95(1–4):405–433
Tang CS, Shi B, Liu C, Zhao LZ, Wang BJ (2008) Influencing factors of geometrical structure of surface shrinkage cracks in clayey soils. Eng Geol 101(3–4):204–217
Tang CS, Shi B, Liu C, Suo WB, Gao L (2011a) Experimental characterization of shrinkage and desiccation cracking in thin clay layer. Appl Clay Sci 52(1–2):69–77
Tang CS, Cui YJ, Shi B, Tang AM, Liu C (2011b) Desiccation and cracking behaviour of clay layer from slurry state under wetting-drying cycles. Geoderma 166(1):111–118
Tang CS, Cui YJ, Tang AM, Shi B (2013) Quantification and characterization of temperature effect on desiccation crack network in soil. Geo-Congress 2013: Stability and Performance of Slopes and Embankments III: pp 762–771
Tang CS, Zhu C, Leng T, Shi B, Cheng Q, Zen H (2019) Three-dimensional characterization of desiccation cracking behavior

of compacted clayey soil using x-ray computed tomography. Eng Geol 255:1–10
Tollenaar RN, van Paassen LA, Jommi C (2017) Observations on the desiccation and cracking of clay layers. Eng Geol 230:23–31
Trabelsi H, Romero E, Jamei M (2018) Tensile strength during drying of remoulded and compacted clay: The role of fabric and water retention. Appl Clay Sci 162:57–68
Vahedifard F, Robinson JD, AghaKouchak A (2016) Can protracted drought undermine the structural integrity of california's earthen levees? J Geotech Geoenviron 142(6):02516001
Vallejo LE Application of fracture mechanics to soils: An overview. In: Fracture Mechanics Applied to Geotechnical Engineering, 1994. ASCE, pp 1–20
van der Meer FP, Moes N, Sluys LJ (2012) A level set model for delamination - modeling crack growth without cohesive zone or stress singularity. Eng Fract Mech 79:191–212
Velazco G, Visalvanich K, Shah SP (1980) Fracture-behavior and analysis of fiber reinforced-concrete beams. Cement Concrete Res 10(1):41–51
Vo TD, Pouya A, Hemmati S, Tang AM (2017) Numerical modelling of desiccation cracking of clayey soil using a cohesive fracture method. Comput Geotech 85:15–27
Vo TD, Pouya A, Hemmati S, Tang AM (2019) Modelling desiccation crack geometry evolution in clayey soils by analytical and numerical approaches. Can Geotech J 56(5):720–729
Wang C, Zhang ZY, Liu Y, Fan SM (2017) Geometric and fractal analysis of dynamic cracking patterns subjected to wetting-drying cycles. Soil till Res 170:1–13
Wang C, Zhang ZY, Qi W, Fan SM (2018a) Morphological approach to quantifying soil cracks: Application to dynamic crack patterns during wetting-drying cycles. Soil Sci Soc Am J 82(4):757–771
Wang JJ, Huang SY, Guo WL, Qiu ZF, Kang K (2020) Experimental study on fracture toughness of a compacted clay using semi-circular bend specimen. Eng Fract Mech 224:106814
Wang JJ, Huang SY, Hu JF (2016) Limit of crack depth in K-IC testing for a clay. Eng Fract Mech 164:19–23
Wang JJ, Zhu JG, Chiu CF, Chai HJ (2007a) Experimental study on fracture behavior of a silty clay. Geotech Test J 30(4):303–311
Wang JJ, Zhu JG, Chiu CF, Zhang H (2007b) Experimental study on fracture toughness and tensile strength of a clay. Eng Geol 94(1–2):65–75
Wang LL, Tang CS, Shi B, Cui YJ, Zhang GQ, Hilary I (2018b) Nucleation and propagation mechanisms of soil desiccation cracks. Eng Geol 238:27–35
Wei X, Gao CY, Liu K (2020) A Review of cracking behavior and mechanism in clayey soils related to desiccation. Adv Civ Eng 2020:8880873
Wei X, Hattab M, Bompard P, Fleureau JM (2016) Highlighting some mechanisms of crack formation and propagation in clays on drying path. Geotechnique 66(4):287–300
Wells AA (1961) Unstable crack propagation in metals: cleavage and fast fracture. Proceedings of the crack propagation symposium 1
Wu HY, Kemeny J, Wu SC (2017) Experimental and numerical investigation of the punch-through shear test for mode ii fracture toughness determination in rock. Eng Fract Mech 184:59–74
Xing XG, Kang DG, Ma XY (2017) Differences in loam water retention and shrinkage behavior: Effects of various types and concentrations of salt ions. Soil till Res 167:61–72
Xu JJ, Zhang H, Tang CS, Cheng Q, Liu B, Shi B (2020) Automatic soil desiccation crack recognition using deep learning. Geotechnique:1–53
Yoshida S, Hallett PD (2008) Impact of hydraulic suction history on crack growth mechanics in soil. Water Resour Res 44:W00C01
Yu Z, Eminue OO, Stirling R, Davie C, Glendinning S (2021) Desiccation cracking at field scale on a vegetated infrastructure embankment. Geotechnique Letters 11(1):88–95
Zeng H, Tang CS, Cheng Q, Inyang HI, Rong DZ, Lin L, Shi B (2019) Coupling effects of interfacial friction and layer thickness on soil desiccation cracking behavior. Eng Geol 260
Zhang B, Hallett PD, Zhang G (2008) Increase in the fracture toughness and bond energy of clay by a root exudate. Eur J Soil Sci 59(5):855–862
Zhang TW, Deng YF, Cui YJ, Lan HX, Zhang FY, Zhang HY (2019) Porewater salinity effect on flocculation and desiccation cracking behaviour of kaolin and bentonite considering working condition. Eng Geol 251:11–23
Zhang Y, Ye WM, Chen B, Chen YG, Ye B (2016) Desiccation of nacl-contaminated soil of earthen heritages in the site of yar city, northwest china. Appl Clay Sci 124:1–10
Zhu XK, Joyce JA (2012) Review of fracture toughness (G, K, J, CTOD, CTOA) testing and standardization. Eng Fract Mech 85:1–46